ASTRONOMY & ASTROPHYSICS
SUPPLEMENT SERIES

SEPTEMBER **1988,** PAGE 385

Astron. Astrophys. Suppl. Ser. **74,** 385-426 (1988)

Isophote shapes of elliptical galaxies. I. The data

R. Bender (*), S. Döbereiner (*) and C. Möllenhoff (*)

Landessternwarte Königstuhl, D-6900 Heidelberg, F.R.G.

Received December 2, 1987; accepted February 23, 1988

Summary. — CCD surface-photometry was carried out for 69 bright elliptical galaxies in the Cousins V, R, I system. This sample contains nearly all elliptical galaxies brighter than $B_T = 12.4$ mag and north of $\delta = -10°$ (47 objects), as well as 22 additional objects selected mostly because of X-ray or radio emission. The data were used to obtain the radial dependence of the surface brightness, ellipticity and major-axis position-angle for each galaxy. The deviations of the isophotes from pure ellipses were analysed for systematic components by means of Fourier transforms. 80 % of the galaxies show systematic deviations larger than 0.2 % in units of the semimajor axis length. Generally the deviations appear in the form of box-shaped or disk-shaped components. The collected data form the basis for a detailed statistical analysis to be described in a forthcoming paper.

Key words : elliptical galaxies — structure of galaxies.

1. Introduction.

In the last few years it has become evident that the isophotes of a large fraction of elliptical galaxies show systematic deviations from pure ellipses (Lauer, 1985 ; Bender and Möllenhoff, 1987 ; Jedrzejewski, 1987). The deviations occur in the form of box-shaped or disk-shaped components.

The particular importance of these deviations was shown by two investigations : Carter (1987) detected weak disk components in some rapidly rotating ellipticals. Bender *et al.* (1987) demonstrated the existence of a striking correlation between box-components and radio emission in elliptical galaxies.

In order to study the frequency of these components and their relations to other morphological and non-morphological parameters, we carried out a detailed isophote analysis for a sample of 69 elliptical galaxies. Here we present the detailed morphological properties of the galaxies : radial profiles in the ellipticity, in the position angle of the major axis, and in the parameters $a(4)/a$ and $a(3)/a$, which are characteristic for the shapes of the isophotes. Especially the relations of the isophote-shape parameters to other global parameters of elliptical galaxies will be the subject of a forthcoming paper.

Section 2 of this paper describes the observations. Section 3 gives the selection criteria and the distribution of absolute magnitudes and ellipticities for the observed galaxies. Section 4 explains the applied reduction procedures. In section 5 we compare our results with published surface photometry. In section 6 we present our data and discuss derived parameters.

2. Observations.

The observations were carried out in June 1985, January 1986 and June 1987 with the CCD camera system of the Landesstern warte Heidelberg attached to the f/8 1.23 m telescope of the German-Spanish Astronomical Center on Calar Alto, Spain. The detector was a red-sensitive GEC P8603/A chip with a pixel size of 22 μm yielding a scale of 0.46 arcsec per pixel and a field of approximately 3×4 arcmin.

Each galaxy was observed in the three Cousins filters V, R and I. The exposure times were chosen such that usually about 80 000 photons per pixel were recorded in the galaxy centers.

3. Observed galaxies.

Our sample comprises 47 elliptical galaxies selected from the Revised Shapley-Ames Catalogue (Sandage and

(*) Visiting Astronomer, German-Spanish Astronomical Center, Calar alto, operated by the Max-Planck-Institut für Astronomie Heidelberg jointly with the Spanish National Commission for Astronomy.

Send offprint requests to : R. Bender.

Tammann, 1981, hereafter RSA) with $B_T < 12.4$ mag and $\delta > -10°$. According to this selection criterion our sample contains about 95 % of all galaxies listed as type E or E/S0 in the RSA. Since the RSA itself is complete to about 85 % at this magnitude limit, our sample contains more than 80 % of all elliptical galaxies north of $\delta = -10°$ and brighter than $B_T = 12.4$ mag.

Table II lists the 47 galaxies contained in this nearly complete subsample of the RSA. Columns 1 to 5 give the NGC numbers of the galaxies, their morphological types according to RSA (Sandage and Tammann, 1981) and to the Second Reference Catalogue of Bright Galaxies (de Vaucouleurs *et al.*, 1976), their total blue magnitudes B_T and their absolute magnitudes M_T according to RSA. Figure 1 and figure 2 show the distributions of ellipticity classes and absolute magnitudes M_T for the RSA-subsample.

Most of the 22 additionally observed galaxies were chosen because of their known radio or X-ray emission. These objects are listed in Table III. Figure 3 and figure 4 show the distributions of ellipticity classes and absolute magnitudes for the total sample, consisting of the galaxies of the RSA-subsample and the additionally observed galaxies.

4. Data Reduction.

First, the standard reduction procedures were applied to the CCD frames. After subtraction of the dark level the variations in pixel efficiency were corrected using the means of several flatfield images taken during twilight.

The flux calibration was done using K-type standard stars matching the colors of elliptical galaxies. From the V magnitudes obtained in this way we estimated B_T magnitudes for some of the galaxies without published B_T-values assuming $B\text{-}V = 0.9$. Because of the fact that the galaxies without published B_T values had small angular sizes compared to the field of the CCD, the determination of the sky level was no problem in these cases. Therefore the B_T derived for these galaxies should be quite reliable (for details see Bender, 1987). Absolute magnitudes were calculated in agreement with RSA, i.e. assuming a uniform Hubble flow with $H_0 = 50$ km/sec/Mpc and a constant distance to the galaxies of the Virgo Cluster corresponding to a mean radial velocity of 1 100 km/s.

The isophote analysis was carried out using a least-squares ellipse fit and a subsequent Fourier analysis described in detail in Bender and Möllenhoff (1987) :

after removal of foreground stars ellipses were fitted to the isophotes. Every isophote was defined by 72 sample points. The coordinates of the sample points were fixed up to fractions of pixels by linear interpolation. Generally about 25 isophotes per image were analysed, covering a range in surface brightness of about 5 mag/sq.arcsec. Outside the central regions of the galaxies median filters were applied in order to increase the signal-to-noise ratio. The sample points defining the isophotes were chosen to be equidistant in the elliptical parameter t, where $x_i = a \cos t_i$ and $y_i = b \sin t_i$. This parametrization yields spatially equidistant sample points, if the ellipse is projected onto a circle. Therefore our method is mathematically equivalent to the method of Carter (1978, 1987). Both methods have the advantage that the subsequently derived Fourier coefficients measuring the deviations of the isophotes from pure ellipses are independent on the ellipticity of the isophote.

In order to detect systematic deviations of the isophotes from pure ellipses, a Fourier analysis was carried out. The radial deviations r_i were expanded in the series :

$$r_i = \sum_{j=0}^{N-1} \alpha_j \cos(t_i\, j) + \beta_j \sin(t_i\, j) .$$

Because of the symmetry of the coefficients

$$\alpha_j = \alpha_{N-j} \quad \text{and} \quad \beta_j = -\beta_{N-j}$$

the deviations are parametrized in the following way :

$$a(j) = \alpha_j + \alpha_{N-j} \quad \text{and} \quad b(j) = \beta_j - \beta_{N-j} .$$

The first five Fourier coefficients $a(0)$, $a(1)$, $a(2)$, $b(1)$, $b(2)$ are equal to zero within the error limits, since they were minimized by the previous ellipse fit. The lowest order deviations from elliptical isophotes, which are symmetric to both axes of the ellipse, are represented by the fourth cosine coefficient $a(4)$. In fact, in nearly all galaxies with significant deviations of their isophotes from pure ellipses $a(4)$ dominated the Fourier spectrum. The effect of a non-zero $a(4)$-coefficient on the isophote shape is shown in figure 5. A positive value of $a(4)$ describes an isophote with a disk component, while a negative value of $a(4)$ corresponds to a box-shaped isophote. Two galaxies typical for both kinds of deviations are displayed in figure 6 and figure 7. Figure 6 shows the elliptical galaxy NGC 4660, which exhibits a disk component. Figure 7 shows the box-shaped elliptical galaxy NGC 5322. In order to have scale-invariant isophote parameters we normalized the Fourier coefficients to the length of the semimajor axis a (see Fig. 13). Since for most of the galaxies the radial changes of the $a(i)$ are not too large, radial averaging of the normalized Fourier coefficients allows to derive single $a(i)/a$ values characteristic for each galaxy.

The errors in ellipticity, position angle and Fourier coefficients were estimated under the assumption, that the deviations of the isophotes from ellipses are solely caused by white noise. If systematic deviations are present, this procedure overestimates the errors. The validity of our error estimate can be inferred from the comparison of the ellipticity, position angle and the Fourier coefficient profiles in the three colors and from the comparison with published surface photometry (see Sect. 5).

The ellipticities, position angles and Fourier coefficients near the centers of the galaxies can also be affected by guiding errors or bad seeing. In these cases the systematic errors could be larger than the estimated errors. However, the parameter values of these inner-

most regions are of no importance for our further considerations.

5. Comparison with published surface photometry.

Since Jedrzejewski (1987) compared in detail his surface photometry with previous work and showed the high accuracy of his results, we confine to the comparison of our measurements with those of Jedrzejewski. Furthermore, only Jedrzejewski (1987) published isophote-shape parameters, which are of similar quality to those obtained here. For comparison we choose NGC 4697, which contains a moderately strong disk component (the usual standard galaxy NGC 3379 shows no significant deviations from purely elliptical isophotes and therefore is not well-suited for our purpose). The profiles in ellipticity, major-axis position-angle and $a(4)/a$ of NGC 4697 are displayed in figure 8 : the measured ellipticities and position angles differ not more than $\Delta(b/a) \simeq 0.01$ and $\Delta \mathrm{P.A.} \simeq 1°$. Because Jedrzejewski's Fourier coefficients refer to the deviations after projecting each isophote to a unit circle, his cos $(4\,\theta)$ components contain as a normalization factor the mean isophote radii. Therefore, before comparing his cos $(4\,\theta)$ components with our $a(4)/a$, the cos $(4\,\theta)$ values have to be multiplied with a factor $\sqrt{b/a}$. From figure 8 it is obvious that the modified cos $(4\,\theta)$ values of Jedrzejewski differ not more than 0.002 from our $a(4)/a$ over the whole radius range between 4 arcsec and 80 arcsec.

6. Results.

The isophote analysis yielded for each galaxy radial profiles of surface brightness, ellipticity, position angle and Fourier coefficients. Figure 13 shows the profiles of ellipticity $(1 - b/a)$, position angle (P.A.) and normalized Fourier coefficients $a(4)/a$ and $a(3)/a$ as functions of the semimajor axis length a. Error bars were calculated using the method of error estimation described in section 4. If the error is smaller than the symbol size, the error bar is omitted. The data points shown in the $a(4)/a$- and $a(3)/a$-profiles are averages over three adjacent isophotes. In nearly all galaxies, $a(4)/a$ is the dominant coefficient. The $a(3)/a$ coefficient is displayed in order to show the significance of the measured $a(4)/a$ value. $a(3)/a$ reflects irregular isophote deviations caused by e.g. dust absorption or tidal deformations.

In order to permit correlation analyses between morphological and non-morphological properties, characteristic parameters were derived for each galaxy in the following way :

1) The effective or half-light radius r_e was evaluated by fitting a de Vaucouleurs law to the surface brightness profiles in linear flux units :

$$F(r) = F_e\, 10^{-3.33((r/r_e)^{1/4} - 1)}$$

where $F(r)$ is the flux of the isophote with the mean radius $r = \sqrt{ab}$, r_e is the mean effective radius and F_e is the flux at r_e. The fit was carried out over a limited range of r to avoid errors due to seeing in the inner regions of the galaxies and due to low signal-to-noise ratio in the outer regions. The surface brightness profiles and their deviations from the de Vaucouleurs law will be discussed in a forthcoming paper.

2) Characteristic values of the ellipticity $(1 - b/a)$ were obtained in the following manner : In case of a peaked ellipticity profile, we choose an ellipticity value near the maximum value, while in case of a continuous increase in ellipticity the value at the de Vaucouleurs radius was selected. The characteristic values of $a(4)/a$ and $a(3)/a$ are means calculated in the following way : The galaxy image was divided in elliptic annulli, each centered around a fitted isophote. Then the $a(4)/a$ and $a(3)/a$ values of each isophote were weighted with the relative flux contribution from the corresponding elliptic annullus and inversely with the noise amplitude. All annulli together covered the whole surface of the galaxy between $2\,r_s$ and $1.5\,r_e$ ($r_s =$ seeing radius, $r_e =$ de Vaucouleurs radius). In order to get a measure of the contribution of the different regions of the galaxies to the averaged values, the summed-up weights of the isophotes in the regions between $2\,r_s$, $0.2\,r_e$, $0.5\,r_e$, r_e and $1.5\,r_e$ are given in table I for NGC 3379, NGC 4278 and NGC 5576.

3) The position angle profiles were used to estimate the isophote twists between the innermost isophote not affected by guiding errors and an outer limit of $1.5\,r_e$. Figure 9 shows the isophote twists of all galaxies as a function of their ellipticities. This diagram confirms the earlier results of Galletta (1980) and Benacchio and Galletta (1980), who found that large twists predominantly occur in galaxies with small ellipticities. There is also good agreement with Galletta's finding that about 8 % of the elliptical galaxies show twists larger than 10°.

Table II gives the characteristic parameters for the RSA-sample, table III those for the additional galaxies. The columns contain the following parameters :

Column 1 : galaxies denoted by their NGC numbers ; column 2 : types according to the Revised Shapley-Ames Catalog (RSA, Sandage and Tammann, 1981) ; column 3 : types according to the 2nd Reference Catalog of Bright Galaxies (de Vaucouleurs *et al.*, 1976) ; column 4 : total blue magnitudes B_T according to RSA or as derived from own CCD photometry ; column 5 : absolute magnitudes M_T calculated using B_T and the distances estimated according to RSA (see above) ; column 6 : FWHM of the seeing of the images ; column 7 : effective or de Vaucouleurs radii r_e in arcsec, the minimum and maximum value of the three values derived from the V, R, I images are given ; column 8 : isophote twists between the innermost radius not affected by seeing or guiding errors and an outer radius of $1.5\,r_e$ in deg. ; column 9 : characteristic ellipticity values, selected as explained in the text ; column 10 : averaged $a(4)/a$ value, the different isophotes are weighted as explained above, the minimum and maximum value of the three values derived from the V, R, I images are given ;

column 11 : averaged $a(3)/a$ value, explanation as in column 10 ; column 12 : an asterisk indicates galaxies with strong dust absorption or strong asymmetric deformations of the isophotes.

Figure 10 shows the relation between our ellipticities and the ellipticity classes according to RSA. Especially for large ellipticities there is a discrepancy between our ellipticities and the ellipticity classes. This is due to the fact, that the ellipticity classes were derived from measurements at comparably large radii, whereas our ellipticities originate from isophotes at smaller radii.

Figures 11 and 12 give the distributions of averaged $a(4)/a$ for the RSA-sample and the total sample respectively. Galaxies with strong dust absorption over a large radius range or significantly asymmetric isophotes (marked with an asterisk in Tab. II and Tab. III) were not included in these histograms. The figures show that boxy isophotes and disk-components occur with similar probability in elliptical galaxies. At least 80 % of all galaxies show significant and systematic deviations from ideal elliptical isophotes.

An extensive discussion of the correlations between he isophote parameter $a(4)/a$ and the other morphological and non-morphological properties of elliptical galaxies will be given in Paper II.

Acknowledgements.

We are grateful to R. Madejsky, F. Ruzicka and the Calar Alto staff for their help and assistance. This research was supported by the Deutsche Forschungsgemeinschaft (SFB 328).

References

BENACCHIO, L., GALLETTA, G. : 1980, *Mon. Not. R. Astron. Soc.* **193,** 885.
BENDER, R., MÖLLENHOFF, C. : 1987, *Astron. Astrophys.* **177,** 71.
BENDER, R. : 1987, Ph. D. thesis (Univ. Heidelberg).
BENDER, R., DÖBEREINER, S., MÖLLENHOFF, C. : 1987, *Astron. Astrophys.* **177,** L53.
BENDER, R., DÖBEREINER, S., MÖLLENHOFF, C. : 1988, in preparation (Paper II).
CARTER, D. : 1978, *Mon. Not. R. Astron. Soc.* **182,** 797.
CARTER, D. : 1987, *Astrophys. J.* **312,** 514.
DE VAUCOULEURS, G., DE VAUCOULEURS, A., CORWIN, H. G., Jr. : 1976, 2nd Reference Catalog of Bright Galaxies (RC2), Texas (University Press) Austin.
GALLETTA, G. : 1980, *Astron. Astrophys.* **81,** 514.
JEDRZEJEWSKI, R. I. : 1987, *Mon. Not. R. Astron. Soc.* **226,** 747.
LAUER, T. R. : 1985, *Mon. Not. R. Astron. Soc.* **216,** 429.
SANDAGE, A., TAMMANN, G. A. : 1981, A Revised Shapley-Ames Catalog of Bright Galaxies (RSA), Carnegie Institute (Washington).

1988A&AS...74..385B

TABLE I. — *Typical weights for the averaging of the Fourier coefficients. The weights of the isophotes are summed up in the regions between the listed radii (r_s = seeing radius, r_e = de Vaucouleurs radius).*

Object \ r	$2r_s$-$0.2r_e$	$0.2r_e$-$0.5r_e$	$0.5r_e$-r_e	r_e-$1.5r_e$
NGC 3379	0.24	0.41	0.24	0.11
NGC 4278	0.21	0.36	0.27	0.16
NGC 5576	0.16	0.41	0.29	0.14

TABLE II. — *The morphological parameters of the nearly complete sample of elliptical galaxies with $B_T < 12.4$ and $\delta > -10°$ selected from the Revised Shapley-Ames Catalog of Galaxies (Sandage and Tammann, 1981).*

(1) Object NGC	(2) (3) TypeType RSA RC2	(4) B_T mag	(5) M_T mag	(6) seeing arcsec	(7) r_e arcsec		(8) ΔPA (°)	(9) 1-b/a	(10) a(4)/a *100		(11) a(3)/a *100		(12) Pec
596	E0 E2P	11.88	-21.15	2.5	16.8	17.1	60	0.08	-0.15	-0.06	-0.06	0.00	
636	E1 E3	12.25	-20.74	1.9	11.0	12.0	15	0.15	0.00	0.13	0.14	0.26	
777	E1 E1	12.23	-22.88	1.8	15.0	15.2	3	0.16	-0.11	-0.07	-0.04	+0.13	
821	E6 E6	11.94	-21.01	1.7	16.7	18.3	0	0.36	1.11	1.21	0.01	0.07	
1052	E3/SO E4	11.53	-20.91	3.8	24.4	28.5	7	0.31	-0.26	-0.06	0.07	0.10	*
1700	E3 E4	11.96	-22.67	4.0	16.6	17.5	2	0.25	0.41	0.55	-0.09	+0.06	
2300	E3 LA	12.14	-21.22	1.7	20.1	20.5	7	0.21	-0.42	-0.36	-0.03	+0.03	
2974	E4 E4	11.78	-21.12	5.0	24.0	?	5	0.35	0.42	0.56	0.23	0.27	
3193	E2 E2	11.80	-20.26	2.0	17.0	17.8	5	0.12	0.21	0.26	0.02	0.11	
3348	E0 E0	12.15	-21.80	1.9	17.8	19.4	5	0.08	0.20	0.39	0.10	0.30	*
3377	E6 E5	11.10	-19.26	1.8	16.1	17.5	0	0.48	0.75	0.86	-0.03	+0.04	
3379	E0 E1	10.33	-20.58	2.4	23.5	24.3	5	0.09	-0.02	+0.17	-0.05	+0.03	
3608	E1 E2	11.88	-19.84	2.1	19.1	19.7	0	0.21	-0.35	-0.12	0.02	0.09	
3610	E5 E5	11.50	-21.33	1.4	7.9	8.2	0	0.39	1.16	1.47	0.13	0.18	
3613	E6 E6	11.60	-21.50	1.3	24.9	25.8	0	0.49	0.20	0.22	-0.19	-0.10	
3640	E2 E2	11.26	-20.60	1.7	35.2	36.7	8	0.21	-0.13	-0.08	-0.01	+0.09	
4125	E6 E6P	10.76	-21.65	2.0	39.6	46.3	0	0.42	0.83	1.07	-0.14	-0.06	
4168	E2 E2	12.20	-19.49	2.3	38.3	39.2	4	0.14	0.43	0.59	-0.06	+0.03	
4261	E3 E2	11.38	-21.71	2.3	25.2	26.7	2	0.22	-1.09	-1.01	0.00	0.09	
4278	E1 E1	11.13	-19.24	2.5	25.0	26.8	15	0.13	0.00	0.09	-0.17	-0.10	*
4291	E3 E2	12.33	-20.75	2.1	8.2	8.7	2	0.25	-0.13	-0.07	-0.17	0.00	
4365	E3 E3	10.60	-21.10	1.9	34.5	37.4	5	0.24	-0.80	-0.70	-0.07	-0.04	
4374	E1 E1	10.23	-21.47	2.2	31.7	32.7	3	0.15	-0.49	-0.42	-0.22	-0.19	
4406	S0/E3 E3	10.02	-21.68	1.9	53.7	54.8	5	0.22	-0.53	-0.47	-0.04	0.00	
4472	E1/S0 E2	9.32	-22.38	2.5	66.4	68.5	5	0.17	-0.23	-0.16	0.04	0.06	
4473	E5 E5	11.07	-20.63	1.6	14.7	15.5	0	0.41	0.76	0.82	-0.17	-0.06	
4478	E2 E2	12.15	-19.55	1.9	25.9	27.4	10	0.17	-0.56	-0.39	-0.07	+0.07	
4494	E1 E1	10.74	-21.27	1.8	28.1	30.2	9	0.16	0.12	0.20	-0.05	-0.03	
4550	E7/S0 LB	12.33	-19.37	1.7	16.2	16.8	0	0.63	1.55	1.79	-0.23	-0.05	
4564	E6 E6	11.87	-19.83	2.0	16.6	17.4	2	0.55	0.59	0.73	-0.07	+0.03	
4589	E2 E2	11.87	-21.36	1.9	29.5	34.6	10	0.19	0.07	0.29	0.09	0.13	*
4621	E5 E5	10.67	-21.03	2.3	27.3	29.3	0	0.34	0.95	1.06	0.07	0.13	
4636	E0/S0 E0	10.50	-20.58	2.4	52.0	54.5	10	0.15	-0.11	-0.01	0.00	0.14	
4649	S0/E2 E2	9.83	-21.87	2.8	48.3	49.6	6	0.17	-0.44	-0.38	-0.05	-0.02	
4660	E5 E5	11.87	-19.83	2.6	9.0	9.8	5	0.45	0.40	0.67	-0.32	-0.14	
4697	E6 E6	10.11	-21.47	2.0	48.5	51.5	0	0.41	0.99	1.08	0.06	0.08	
4742	E4 E4	12.11	-19.63	2.9	2.7	3.6	0	0.37	0.34	0.48	-0.11	+0.03	
5322	E4 E3	10.91	-22.04	1.6	24.9	26.0	2	0.31	-0.37	-0.30	-0.07	0.00	
5557	E2 E1	12.01	-22.08	1.8	18.9	19.3	5	0.18	-0.15	-0.07	0.08	0.10	
5576	E4 E3	11.76	-20.51	1.8	11.7	11.9	0	0.30	-0.58	-0.41	0.00	0.11	
5638	E1 E1	12.20	-20.31	2.3	25.0	25.9	15	0.09	0.04	0.09	0.03	0.14	
5812	E0 E0	12.33	-20.68	2.1	12.8	13.5	5	0.05	0.00	0.12	-0.05	+0.14	
5813	E1 E1	11.61	-21.21	1.7	22.0	22.7	10	0.15	0.04	0.10	-0.36	-0.23	*
5982	E3 E3	12.08	-21.89	3.1	14.0	14.4	0	0.29	-0.48	-0.45	-0.13	-0.01	
6482	E2 E3	12.10	-22.66	2.3	17.7	20.6	7	0.25	0.60	0.79	0.00	0.06	
7619	E3 E2	12.21	-22.36	2.0	13.8	15.5	0	0.21	0.18	0.30	-0.04	+0.02	
7626	E1 E1P	12.21	-22.13	1.7	27.1	30.4	10	0.15	0.11	0.13	-0.22	-0.16	*

TABLE III. — *The morphological parameters of the additionally observed galaxies, selected mostly because of their known radio or X-ray emission.*

(1) Object NGC	(2) (3) TypeType RSA RC2	(4) B_T mag	(5) M_T mag	(6) seeing arcsec	(7) r_e arcsec		(8) ΔPA (°)	(9) 1-b/a	(10) a(4)/a *100		(11) a(3)/a *100		(12) Pec
315	E LA	12.20	-22.90	3.6	33.5	34.8	2	0.25	-0.40	-0.22	-0.20	-0.12	
584	S0(4) E4	11.20	-21.80	2.9	21.8	22.4	2	0.35	0.28	0.30	-0.10	+0.02	
890	S0(5) LXR	12.26	-22.40	2.3	19.9	20.5	0	0.38	-0.70	-0.62	0.11	+0.16	
1199	E2 E3	12.42	-21.23	2.4	17.9	20.1	1	0.24	-0.48	-0.43	-0.15	+0.05	
3607	S0(3) LAS	11.08	-20.02	2.3	23.9	26.7	2	0.20	-0.22	-0.03	-0.24	-0.08	*
3842	E E3	13.20	-22.20	2.6	20.0	22.4	7	0.18	-0.33	-0.07	-0.16	+0.06	
3894	E E4	12.60	-21.50	1.8	19.4	21.6	0	0.39	-0.44	-0.29	0.01	0.08	
3923	E4/S0 E4	10.91	-21.61	3.6	41.3	42.6	0	0.35	-0.20	-0.17	0.00	0.04	
4251	S0(8) LB	11.62	-19.82	1.7	24.1	24.8	2	0.50	1.71	1.98	-0.16	-0.02	
4382	S0(3)p LAS	10.10	-21.60	2.9	31.5	35.9	2	0.20	0.46	0.68	-0.02	+0.07	
4552	S0(0) E0	10.80	-20.90	2.0	21.9	22.9	22	0.06	-0.03	+0.07	-0.20	-0.12	
4889	E4 E4	12.57	-22.99	2.1	19.4	20.0	2	0.34	-0.14	+0.04	-0.27	-0.14	*
5127	E2	13.00	-21.90	1.7	26.4	28.6	3	0.24	-0.60	-0.42	0.00	0.05	
14296	E0 E0	11.58	-22.72	2.3	19.0	20.0	4	0.09	-0.19	0.00	0.02	0.07	
5444	E3 LA	12.50	-22.01	1.6	15.6	16.5	6	0.18	-0.04	+0.12	0.00	0.21	
5490	E2 E2	12.80	-22.20	2.0	9.7	10.0	3	0.18	0.21	0.34	-0.05	+0.06	
5831	E4 E3	12.50	-20.07	1.9	19.4	20.0	21	0.23	0.39	0.43	-0.04	+0.09	
6251	13.30	-22.50	1.7	13.3	14.1	0	0.15	0.07	0.23	0.31	0.41	*	
7052	E4	12.70	-22.40	2.6	20.8	23.8	0	0.48	-0.15	-0.05	0.11	0.20	
7385	E1P	13.20	-22.80	3.2	30.4	31.6	10	0.13	-0.15	+0.03	0.13	0.19	
7562	E E2	12.50	-22.00	2.5	17.5	17.9	1	0.28	-0.19	-0.09	-0.06	+0.03	
7785	E5 E5	12.67	-21.87	2.5	18.4	19.5	0	0.40	-0.72	-0.71	0.20	0.25	

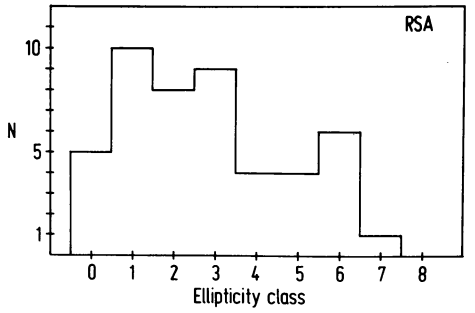

FIGURE 1. — Distribution of the ellipticity classes for nearly all elliptical galaxies of the Revised Shapley-Ames catalog (Sandage and Tammann, 1981) with $B_T < 12.4$ and $\delta > -10°$ (RSA subsample).

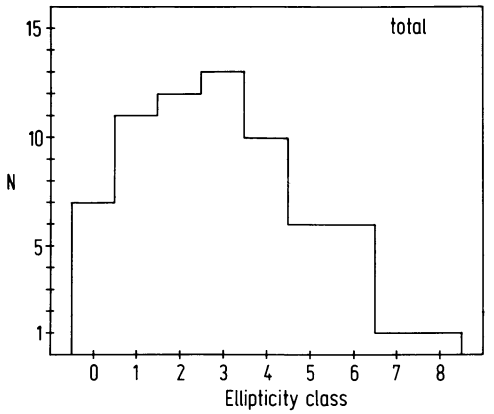

FIGURE 3. — Distribution of the ellipticity classes for all observed elliptical galaxies.

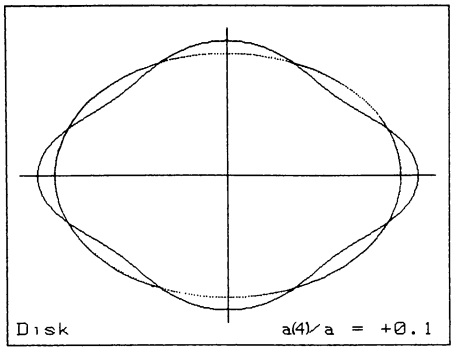

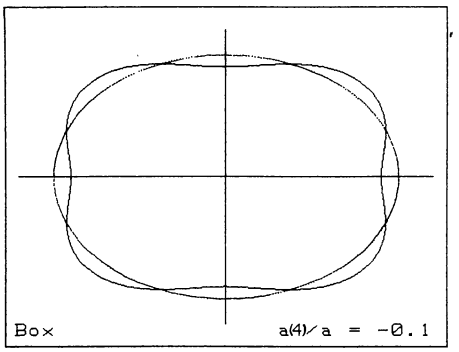

FIGURE 5. — Schematic drawing illustrating isophotes with $a(4)/a = +0.1$ and $a(4)/a = -0.1$.

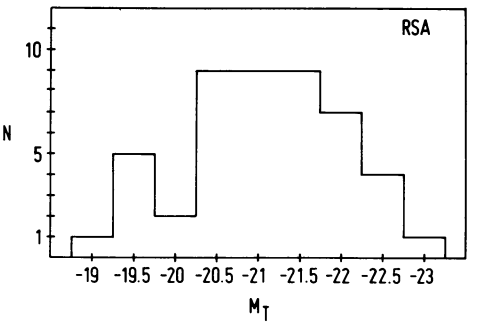

FIGURE 2. — Distribution of the absolute magnitudes for the RSA subsample (see Fig. 1).

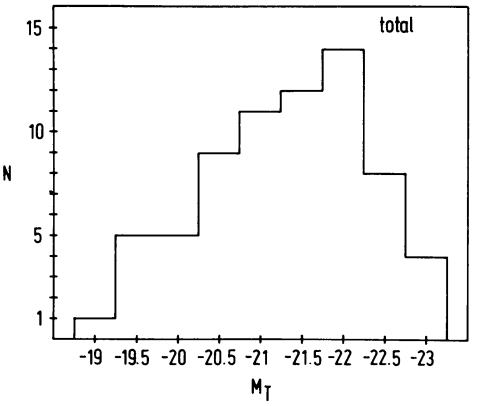

FIGURE 4. — Distribution of the absolute magnitudes for all observed elliptical galaxies.

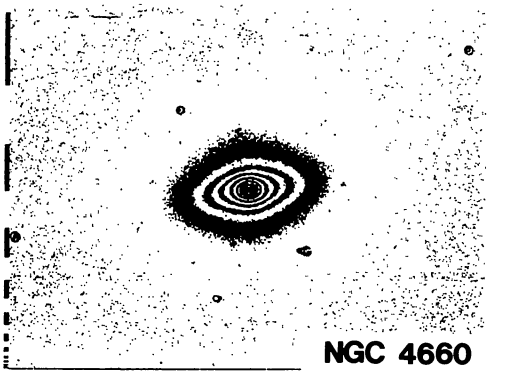

FIGURE 6. — R-image of NGC 4660, an elliptical galaxy with a disk-component in the isophotes ($a(4)/a \sim +0.03$).

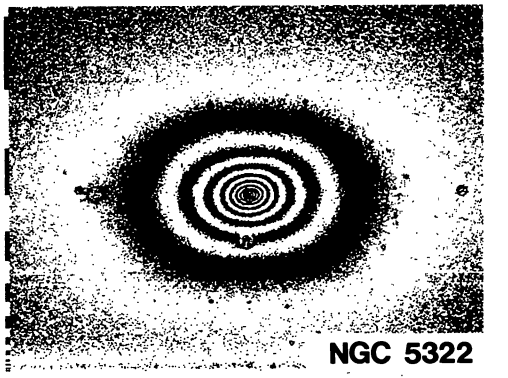

FIGURE 7. — R-image of NGC 5322, an elliptical galaxy with box-shaped isophotes ($a(4)/a \sim -0.01$).

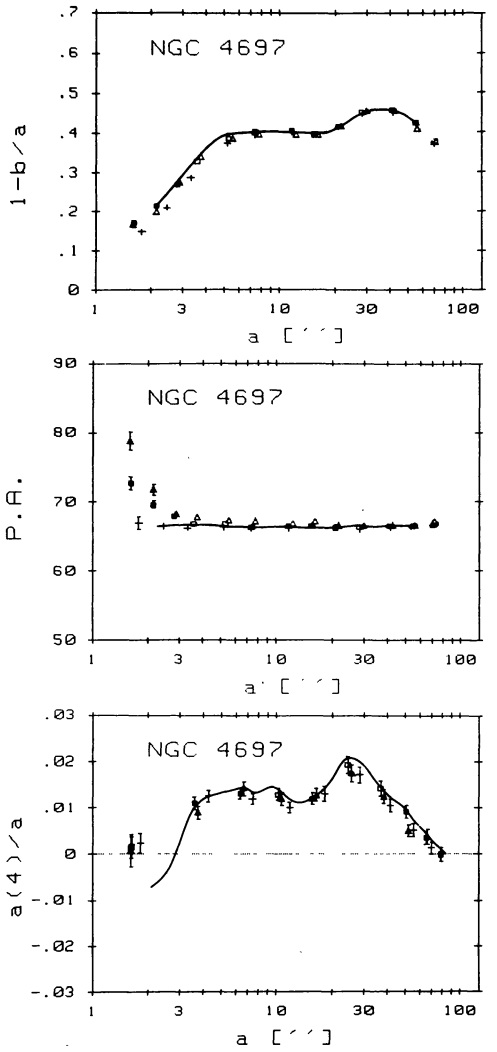

FIGURE 8. — The ellipticity $1 - b/a$, the major-axis position-angle P.A. and the normalized $a(4)/a$ as functions of the semimajor axis a for NGC 4697. The crosses, triangles and squares are values derived from V, R, I images obtained for this investigation. The solid lines give the data as obtained by Jedrzejewski (1987).

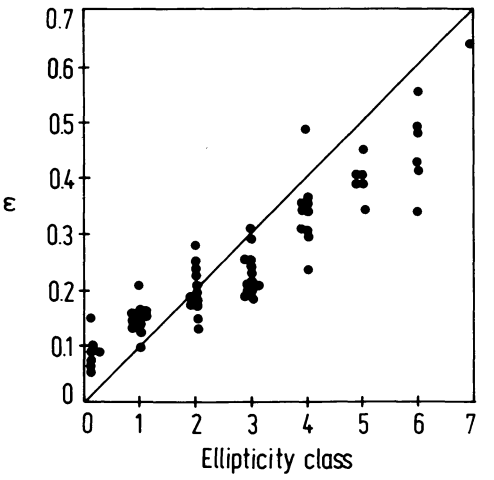

FIGURE 10. — The ellipticities (see text) as a function of the ellipticity class.

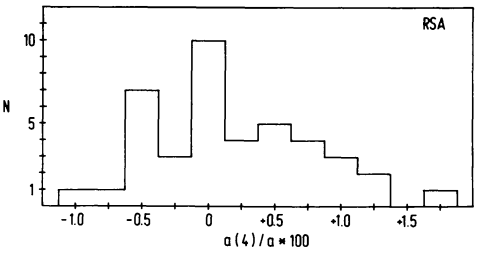

FIGURE 11. — The distribution of the mean $a(4)/a$ measuring the deviations of the isophotes from pure ellipses for the nearly complete sample of elliptical galaxies with $B_T < 12.4$ and $\delta > -10°$.

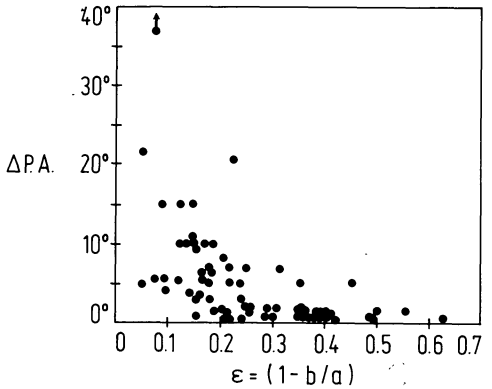

FIGURE 9. — The isophote twists between the innermost isophote not affected by seeing or guiding errors and 1.5 r_e (r_e = de Vaucouleurs radius) as a function of the ellipticities for all galaxies observed.

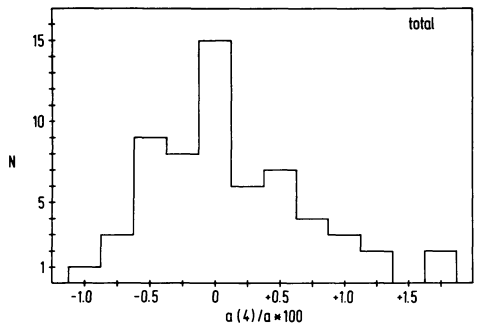

FIGURE 12. — The distribution of the $a(4)/a$ measuring the deviations of the isophotes from pure ellipses for all elliptical galaxies observed.

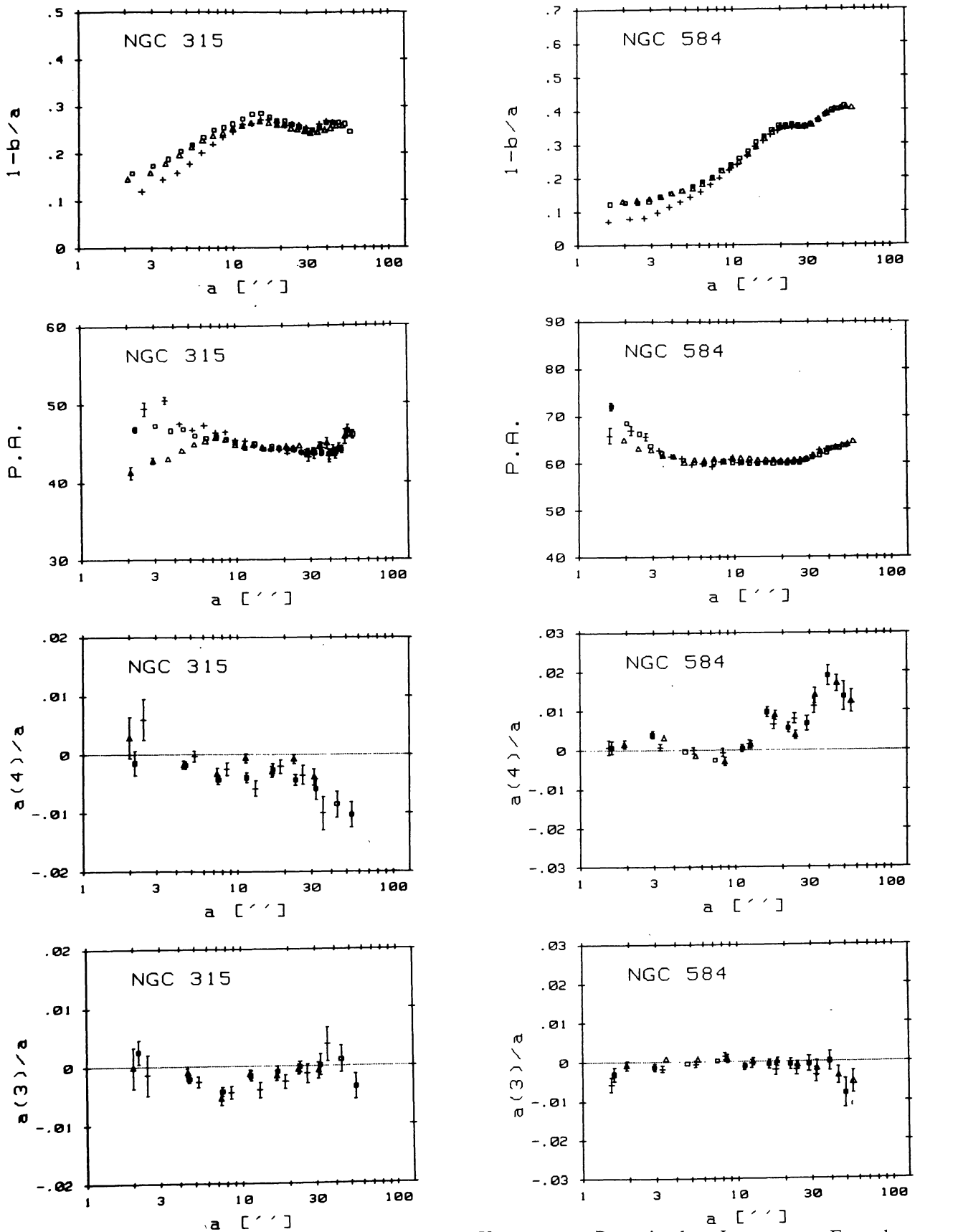

FIGURE 13. — The ellipticities, major-axis position-angles and normalized Fourier coefficients $a(4)/a$ and $a(3)/a$ as functions of the semimajor axis length a for all observed galaxies. The results of different colors are represented by different symbols : $V =$ crosses, $R =$ triangles, $I =$ squares. Error bars are omitted, if they are smaller than the symbol size. Because of an offset error, for NGC 1700 and NGC 2974 only relative position angles could be plotted.

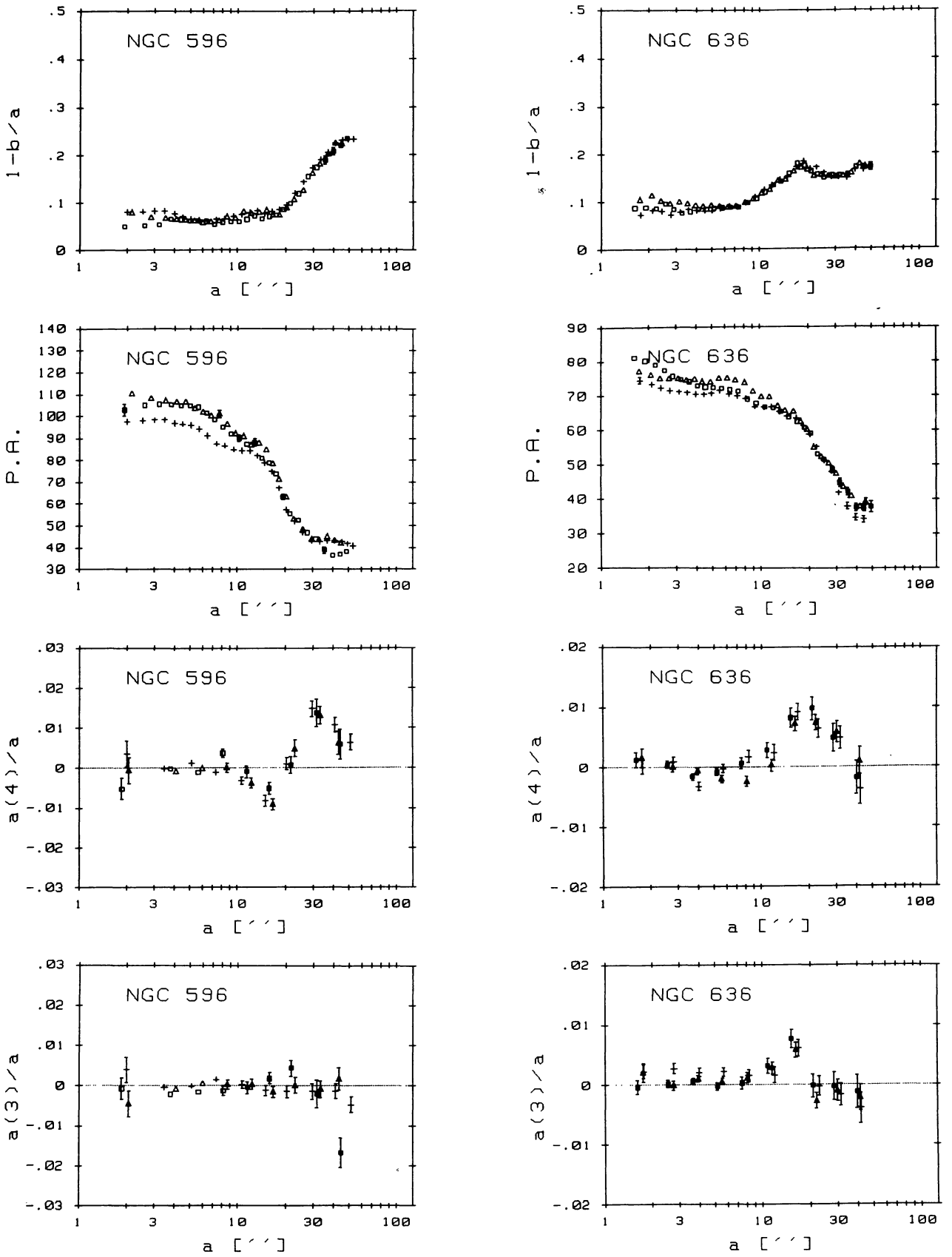

FIGURE 13 *(continued).*

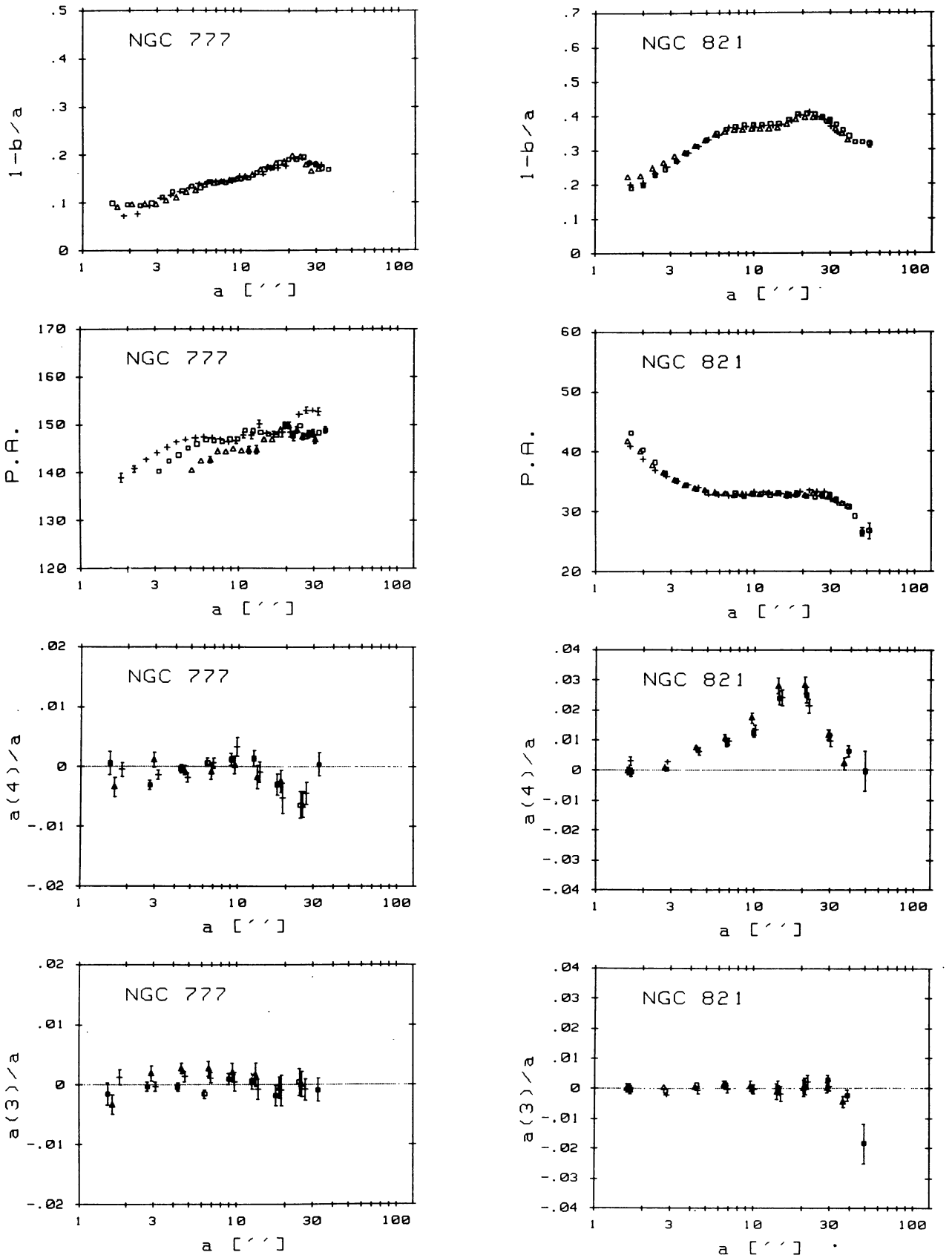

FIGURE 13 *(continued).*

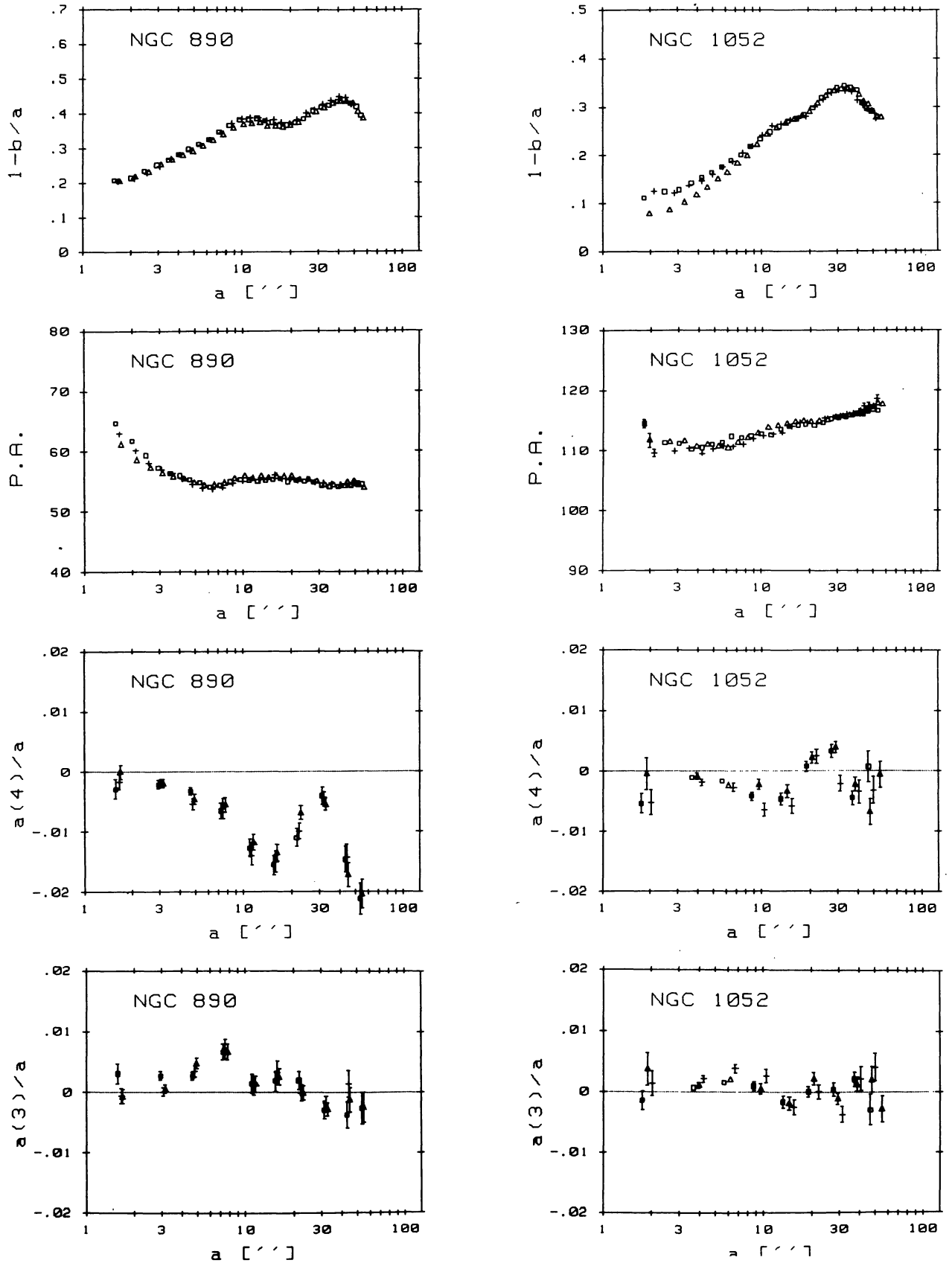

FIGURE 13 *(continued).*

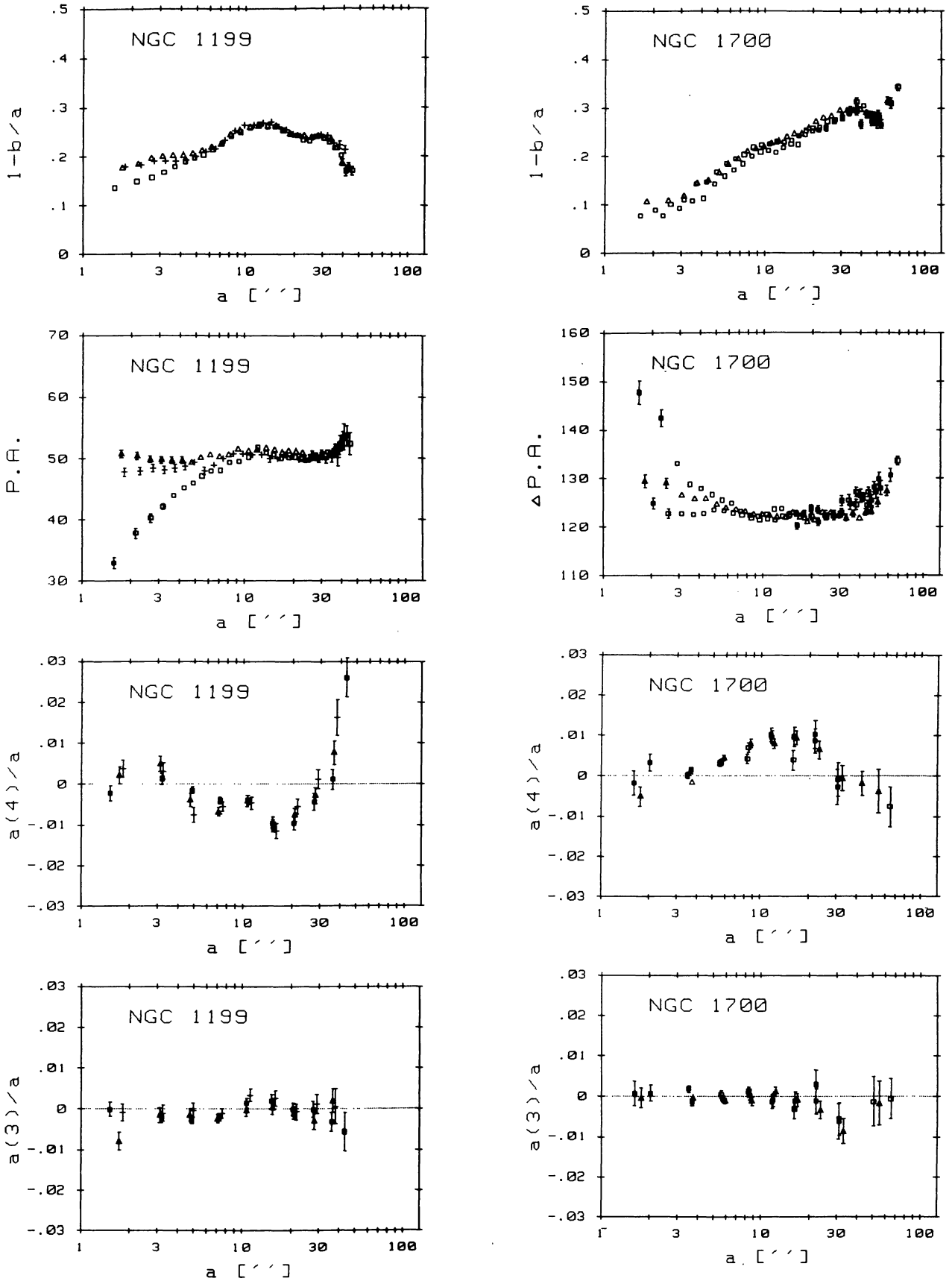

FIGURE 13 *(continued).*

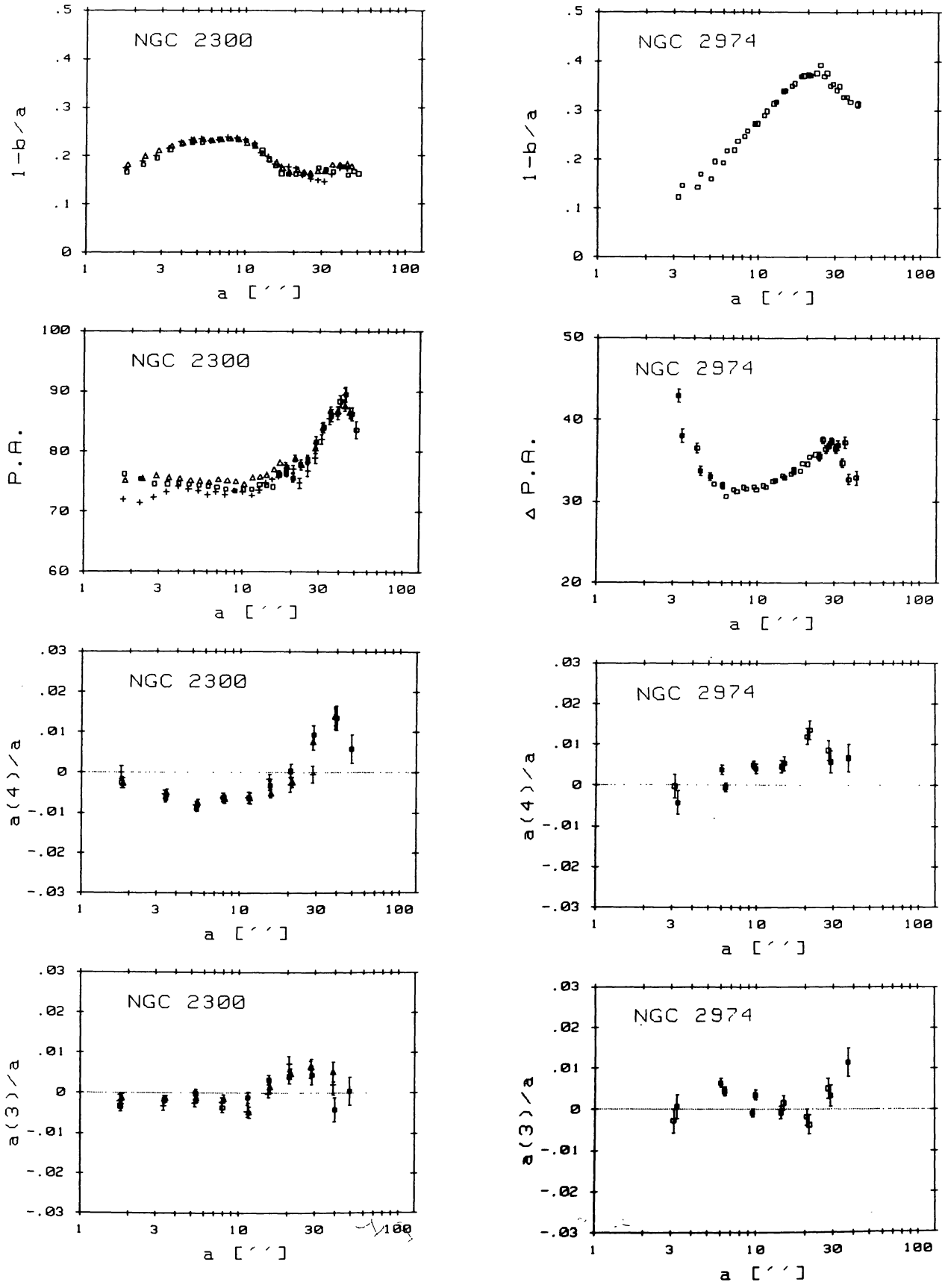

FIGURE 13 *(continued).*

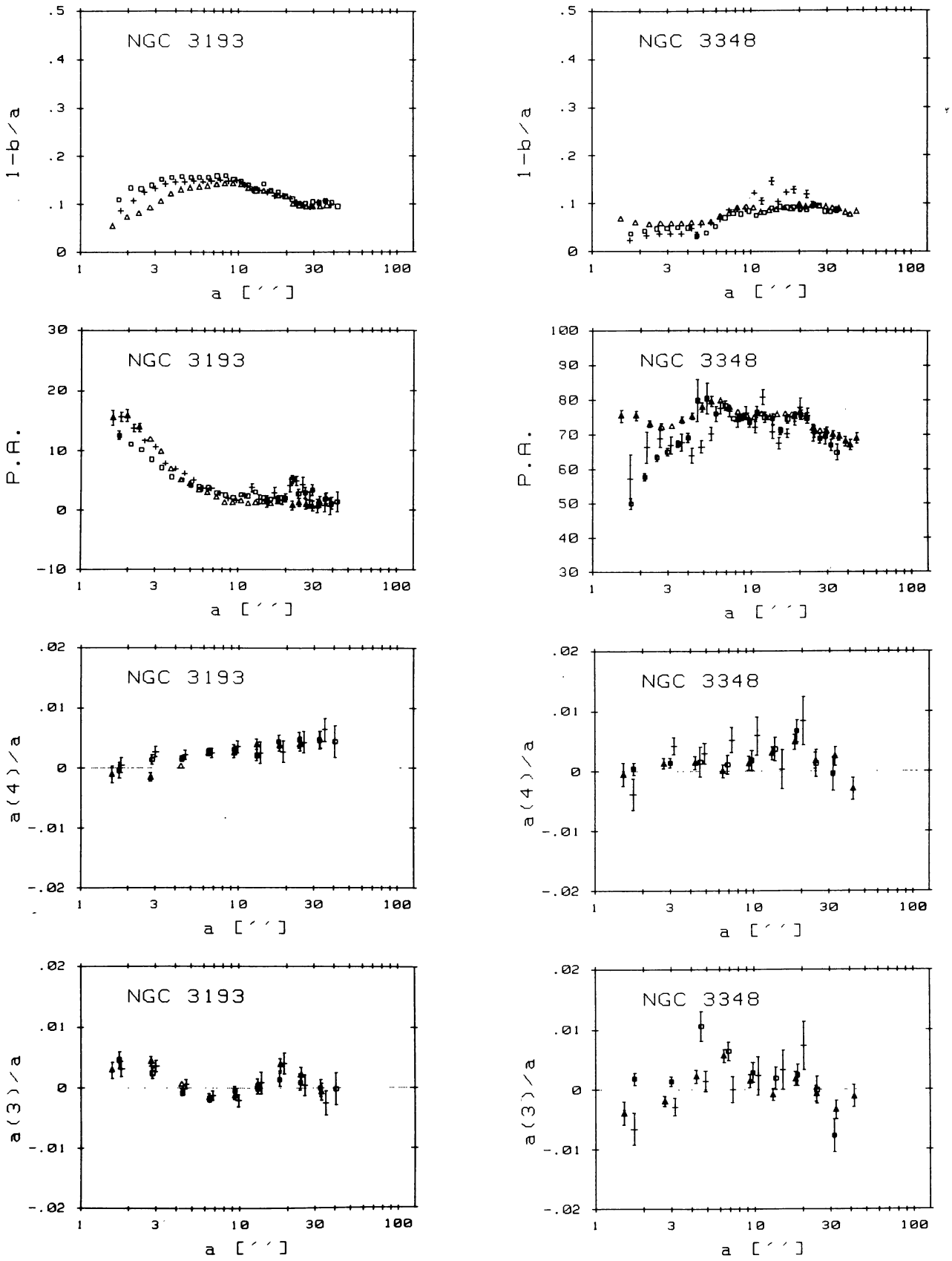

FIGURE 13 *(continued).*

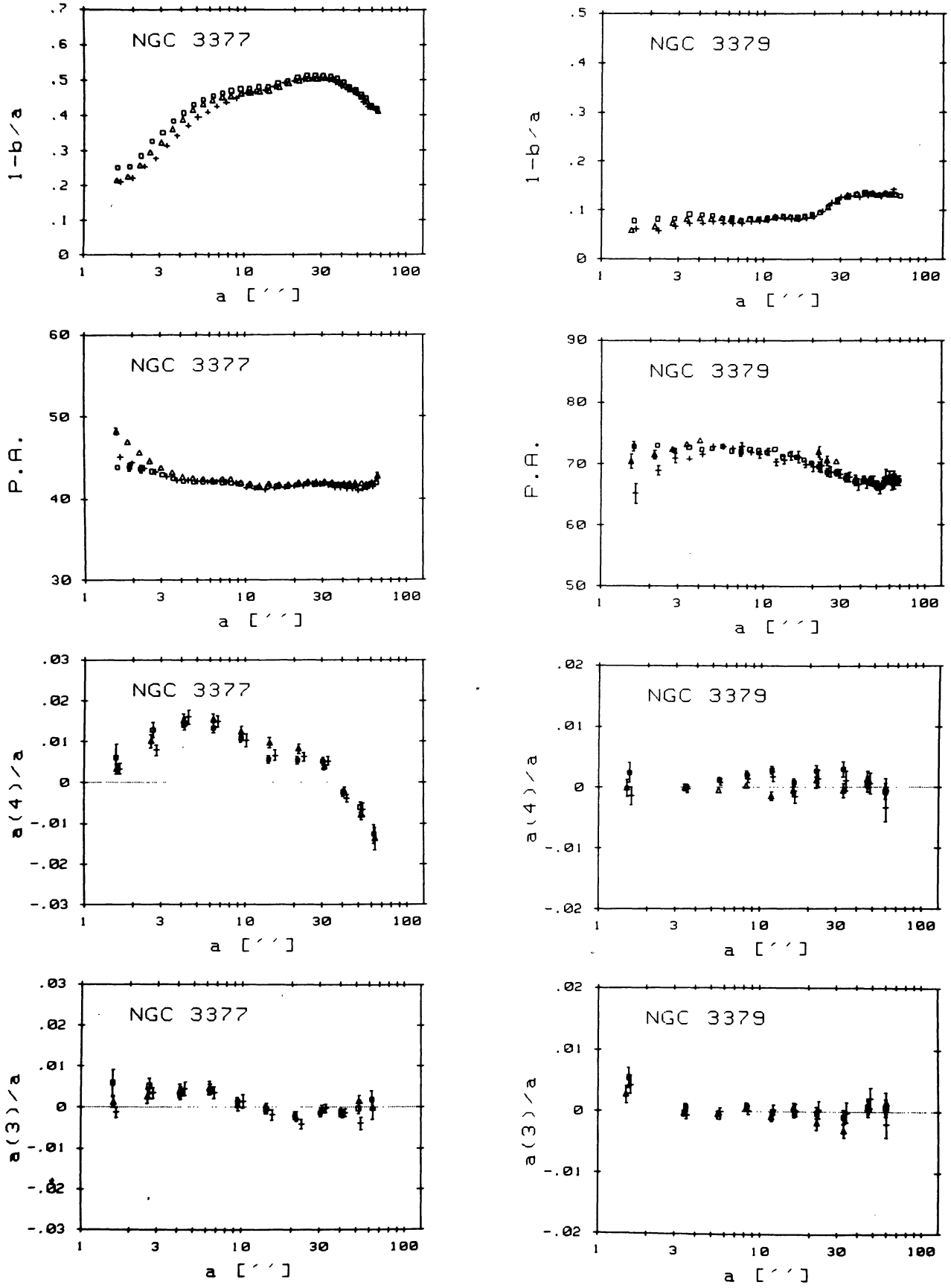

FIGURE 13 *(continued).*

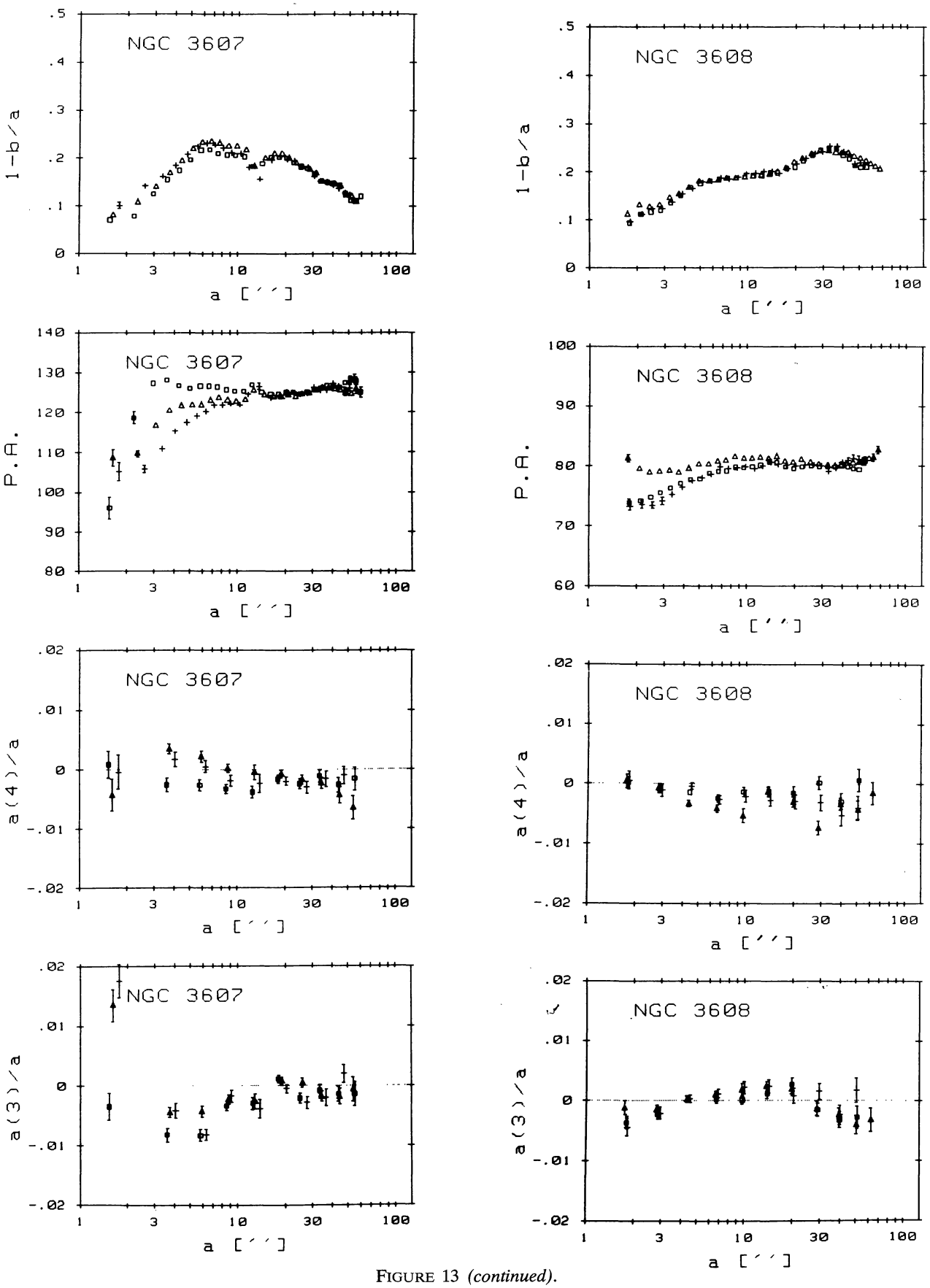

FIGURE 13 *(continued).*

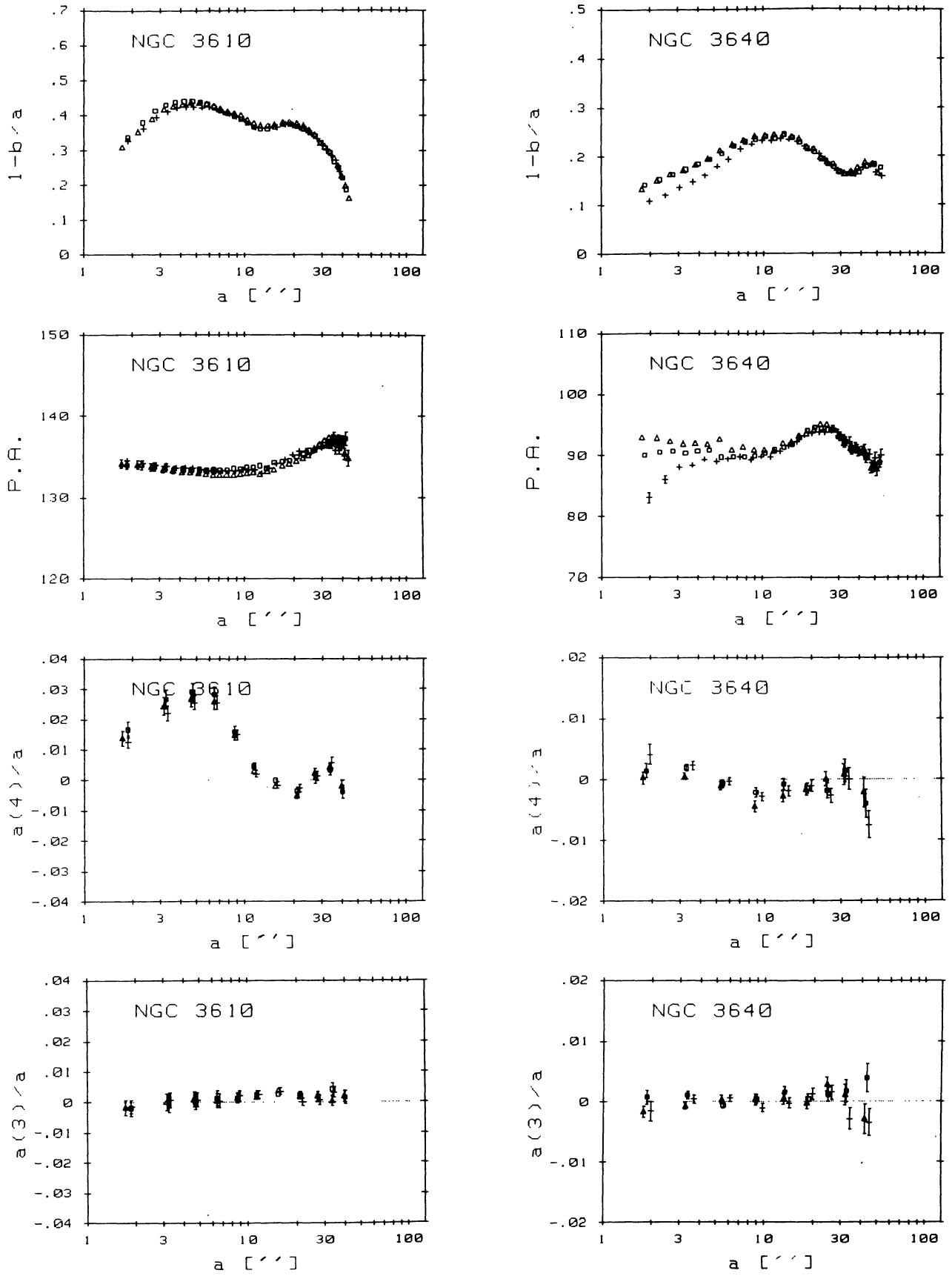

FIGURE 13 *(continued)*.

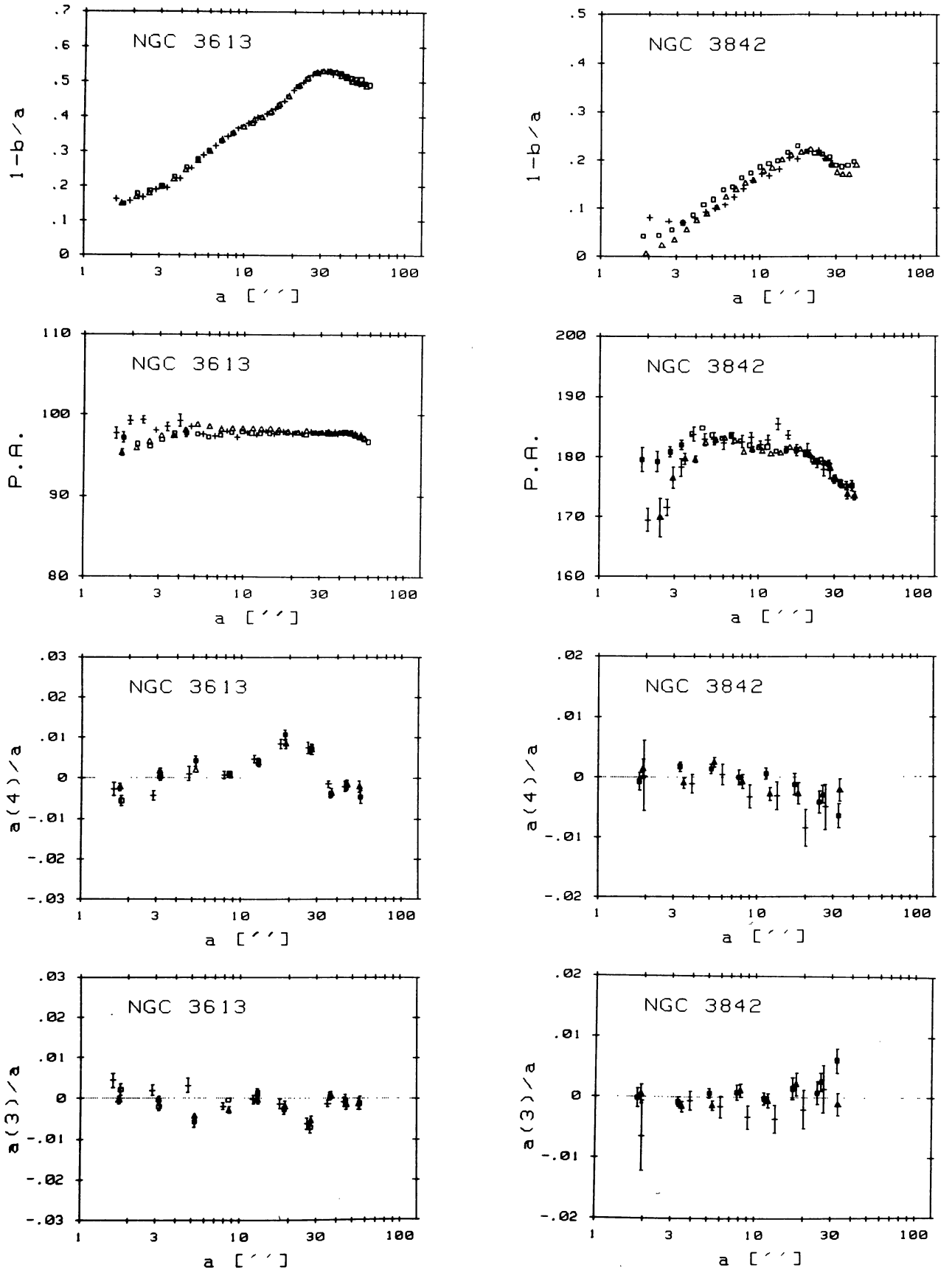

FIGURE 13 *(continued).*

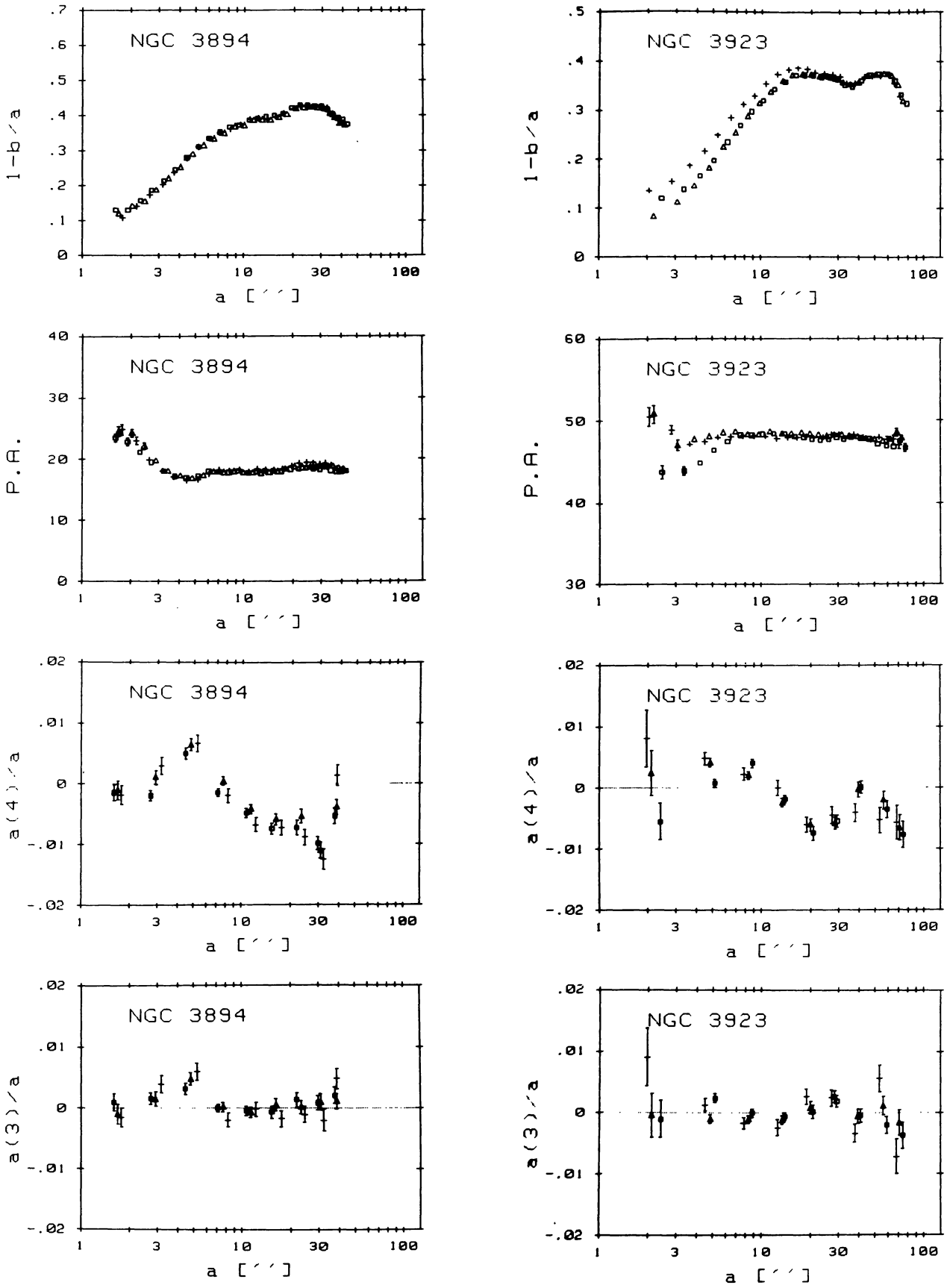

FIGURE 13 *(continued).*

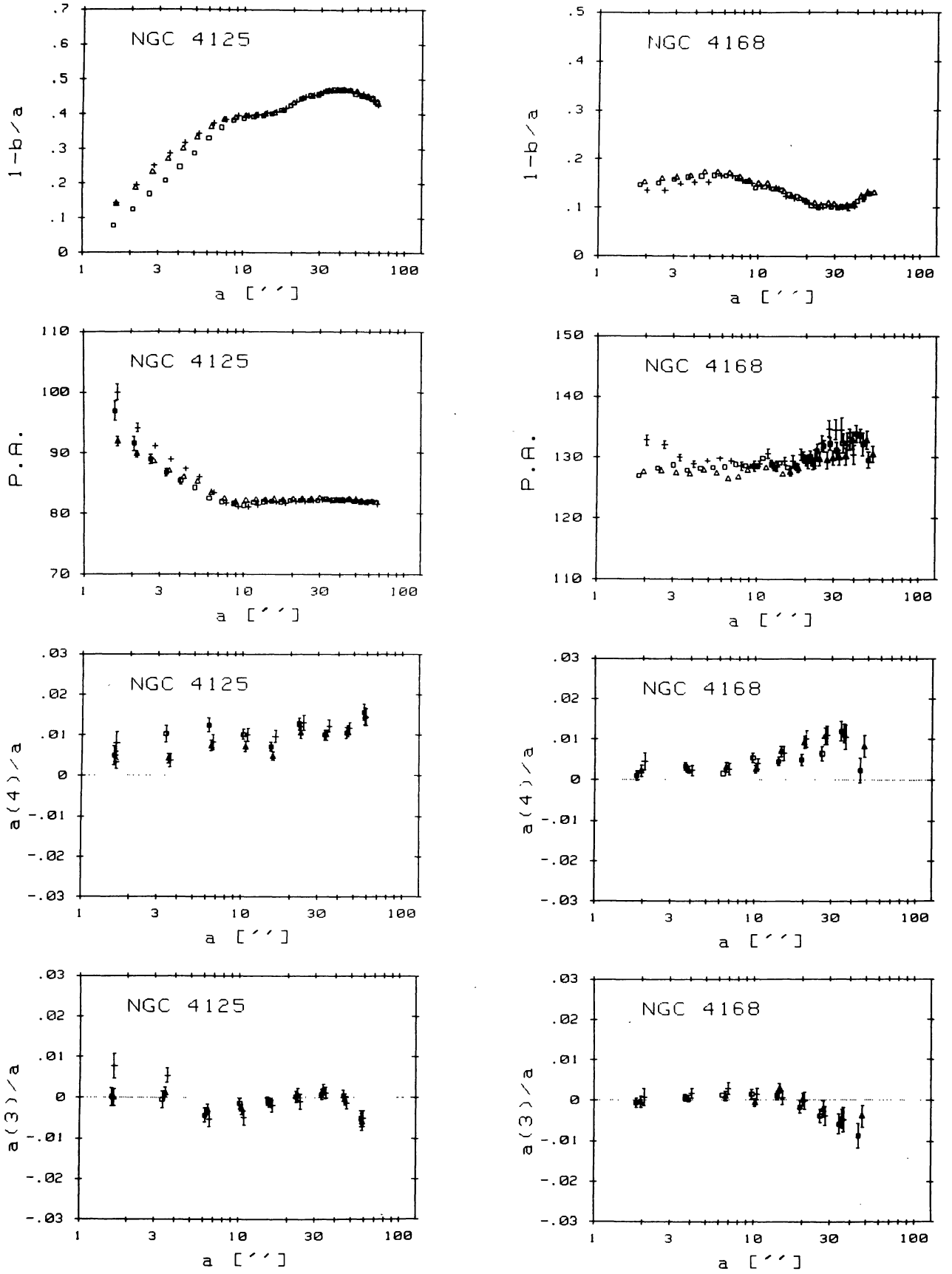

FIGURE 13 *(continued).*

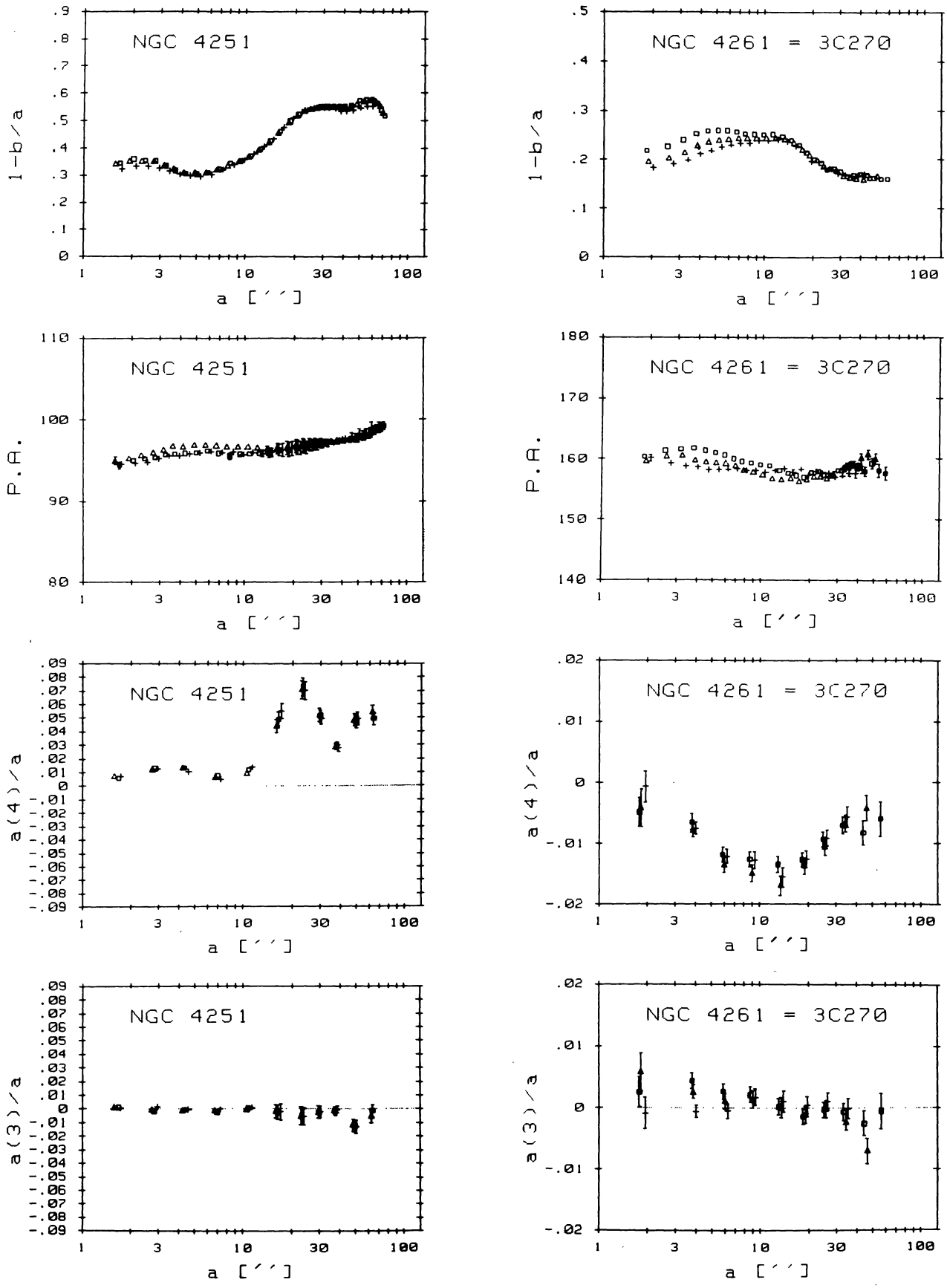

FIGURE 13 *(continued).*

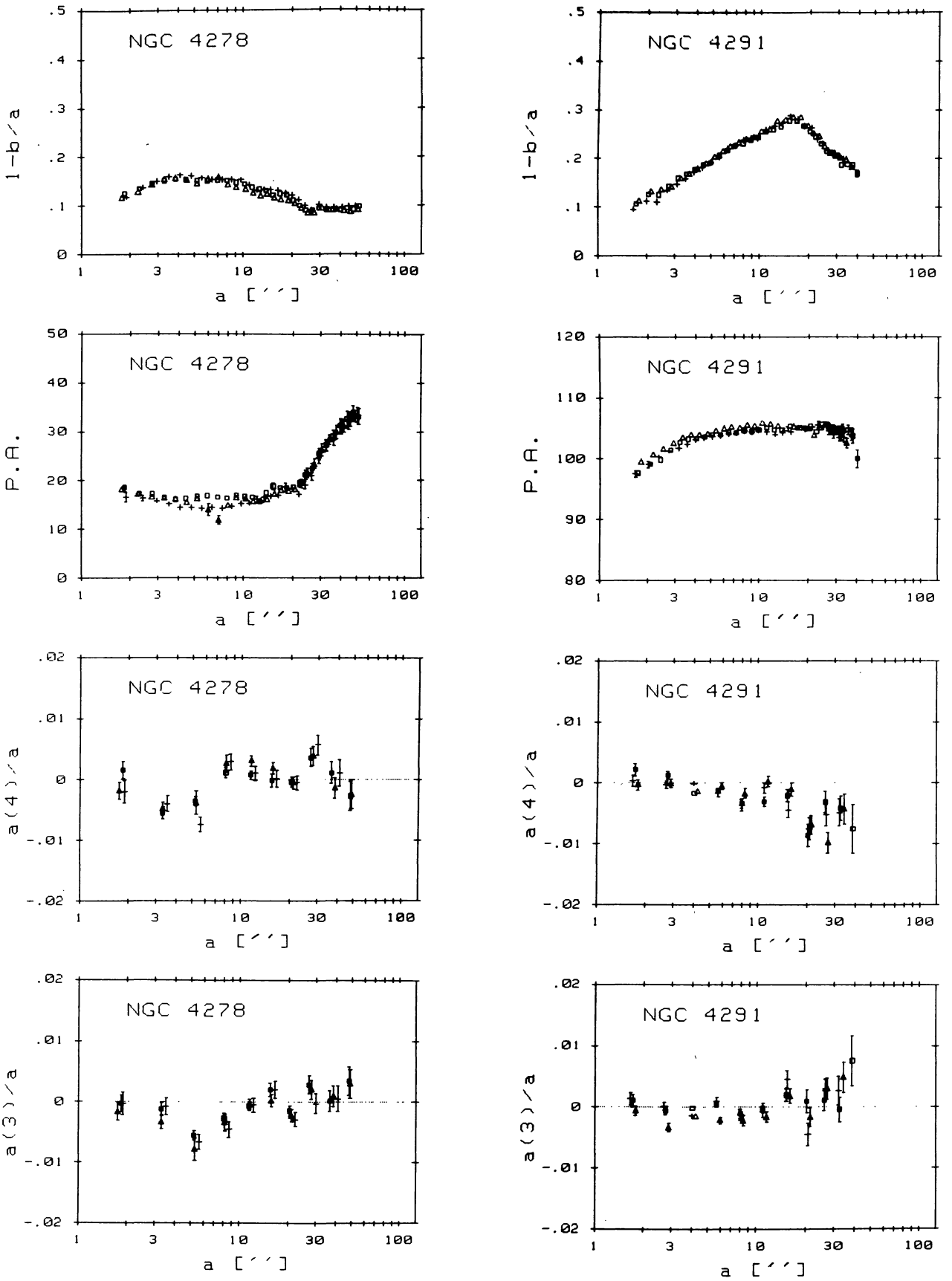

FIGURE 13 *(continued).*

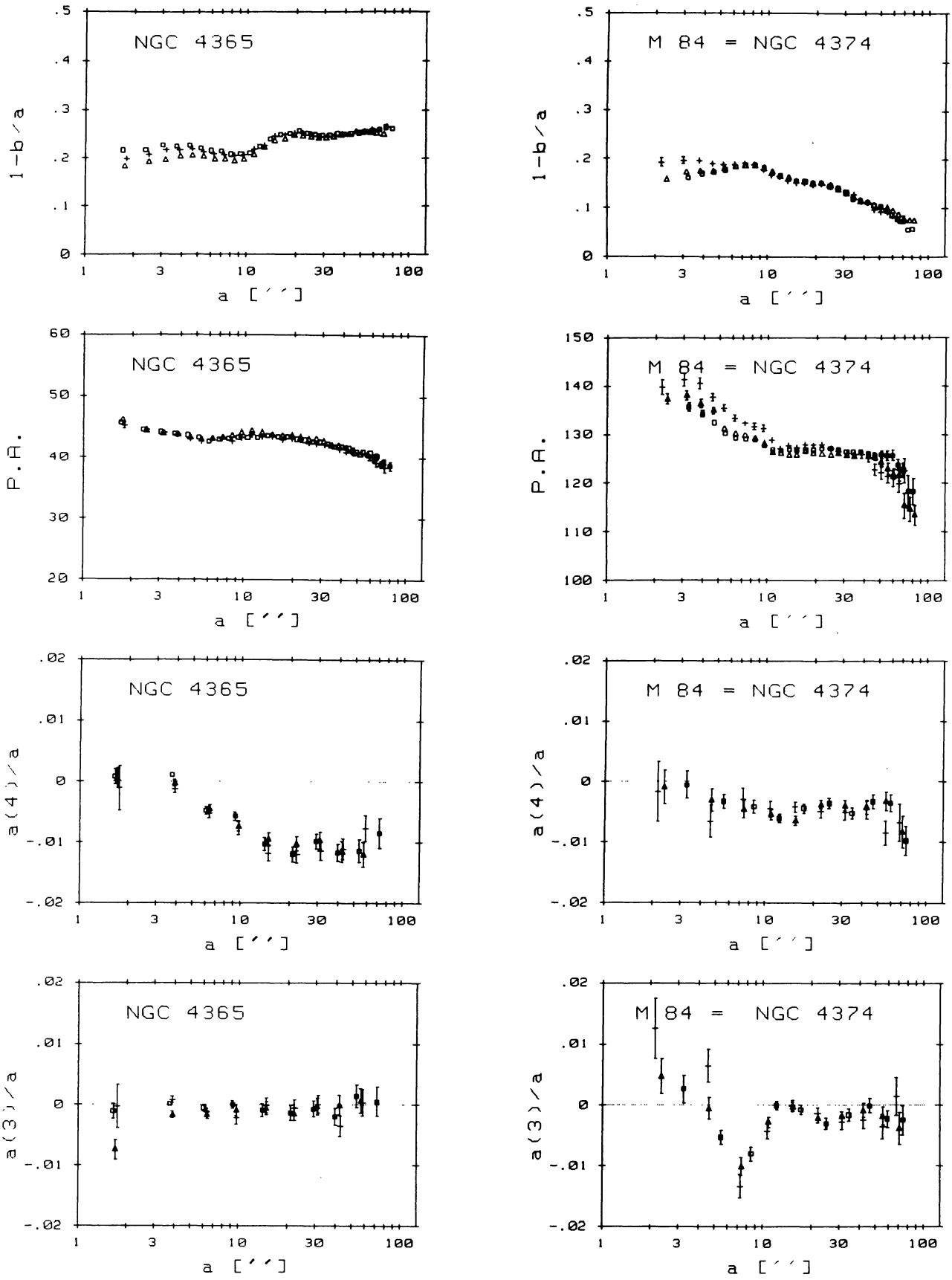

FIGURE 13 *(continued).*

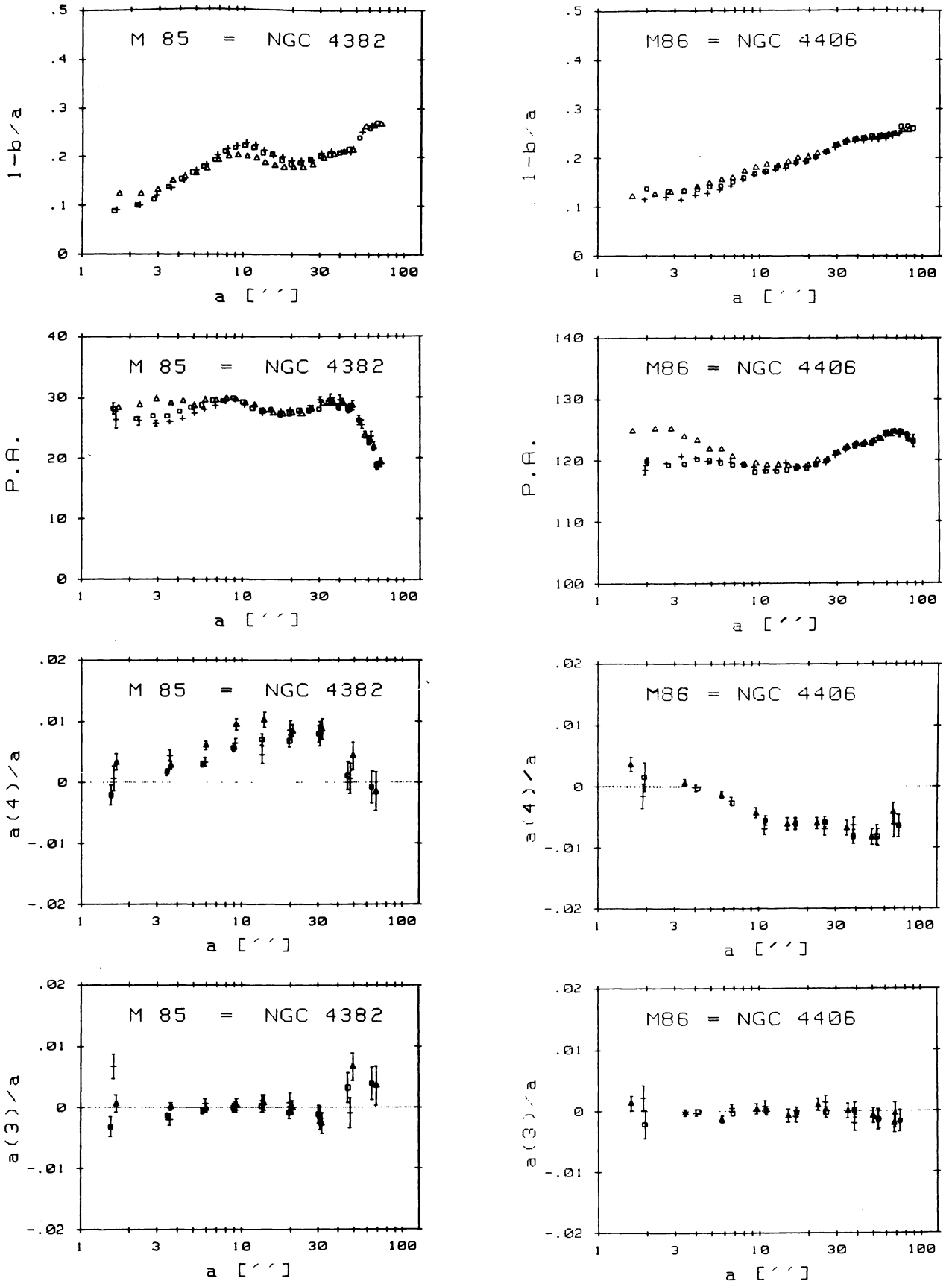

FIGURE 13 *(continued).*

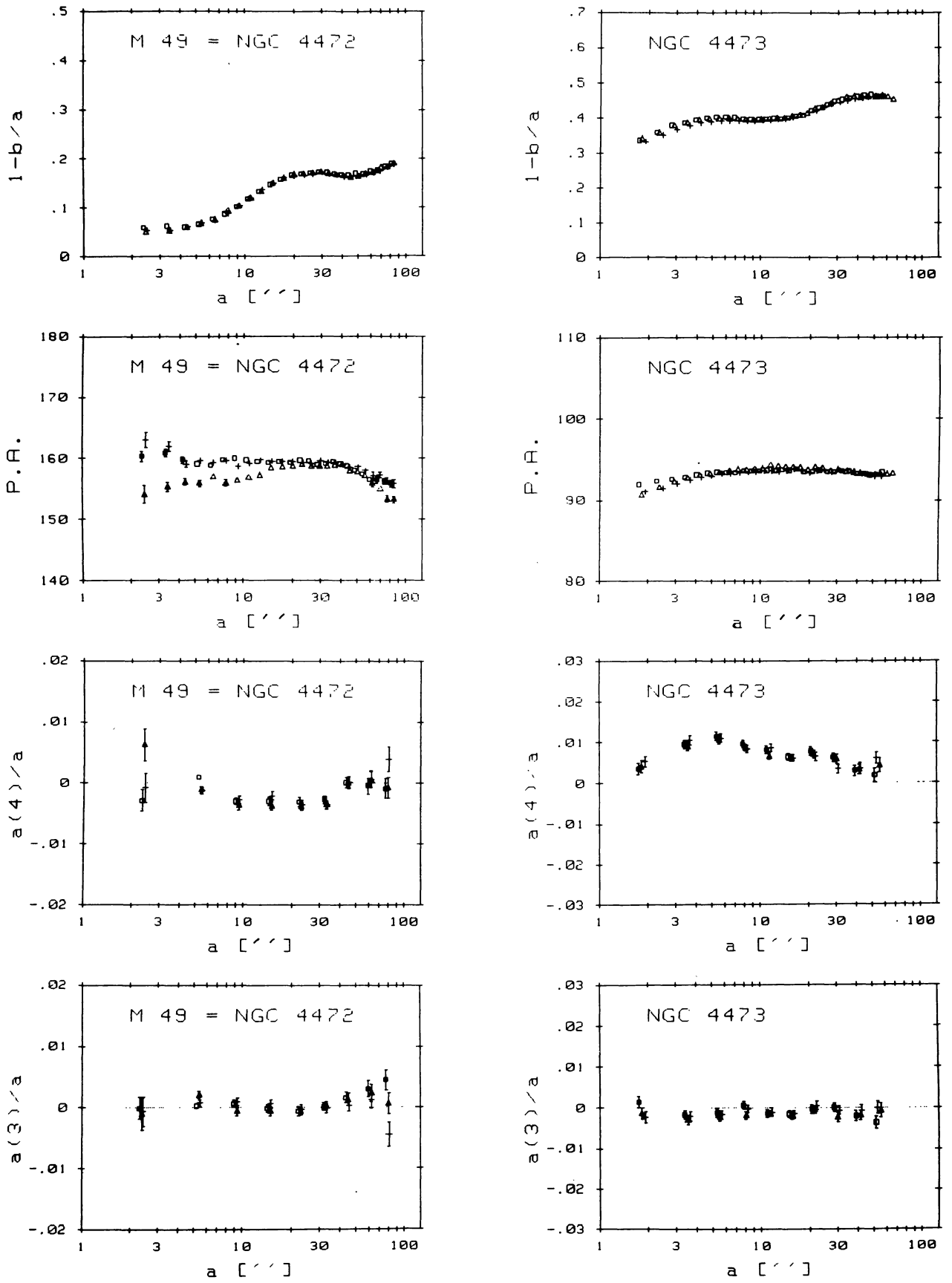

FIGURE 13 *(continued).*

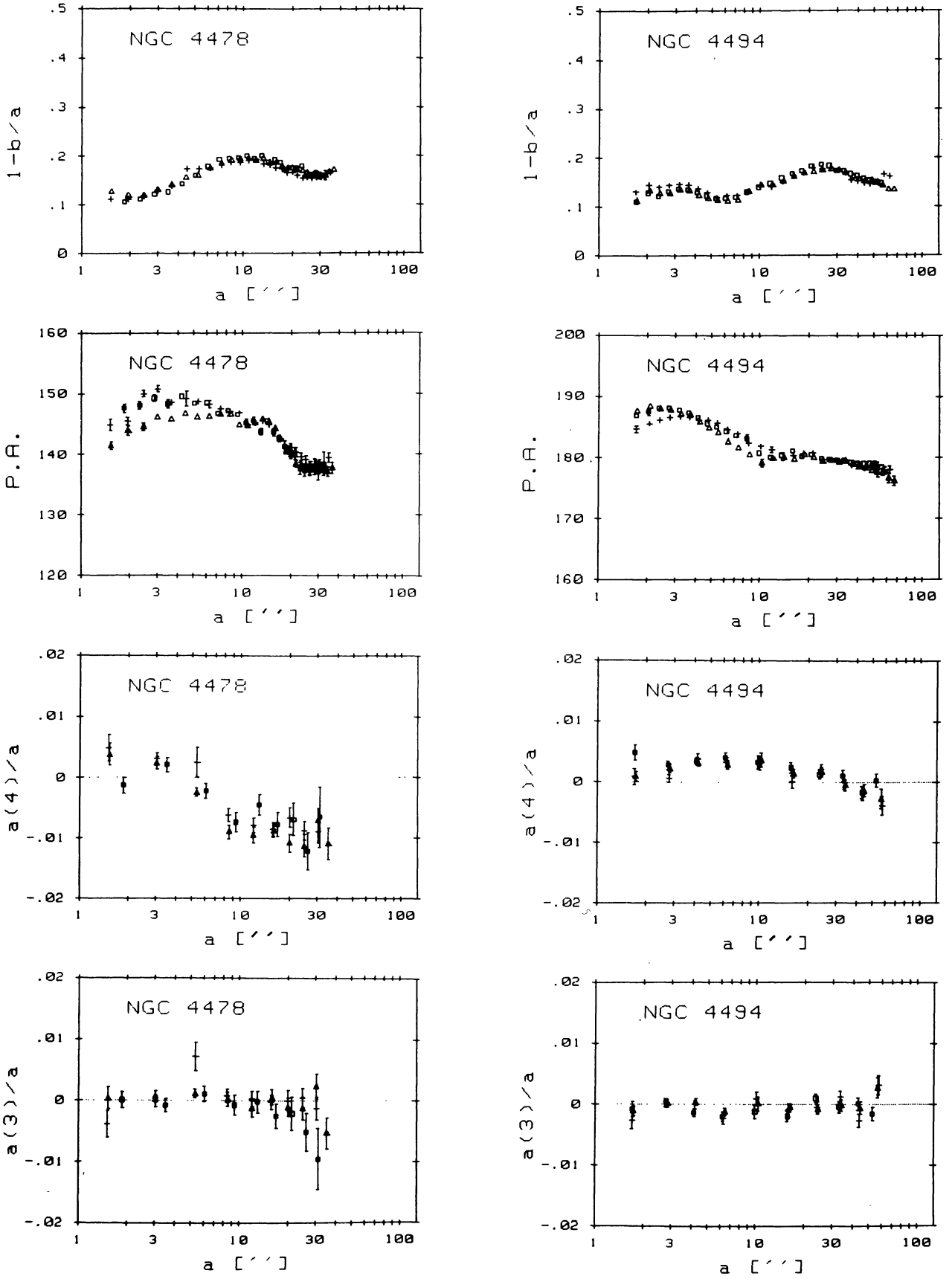

FIGURE 13 *(continued).*

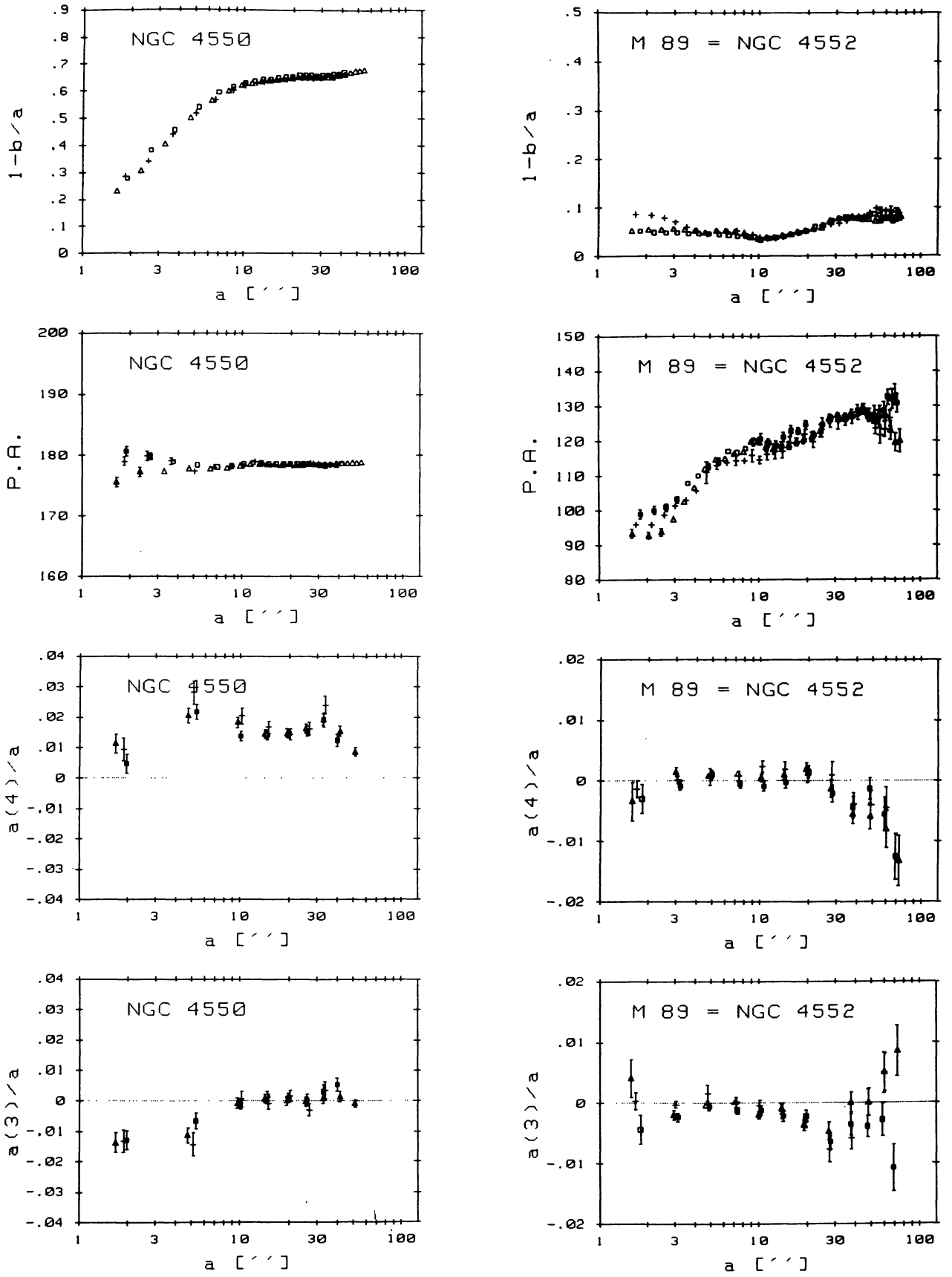

FIGURE 13 *(continued).*

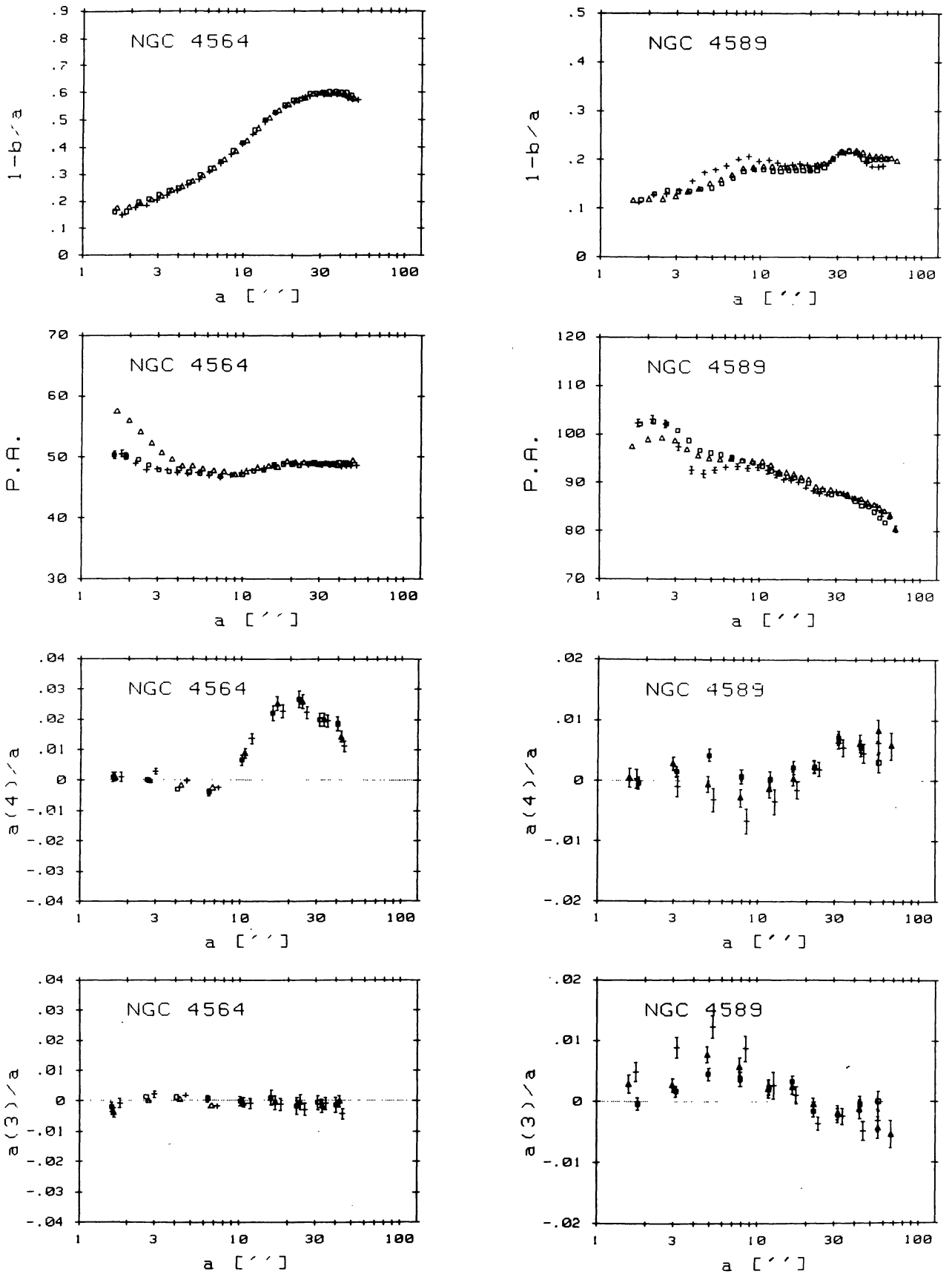

FIGURE 13 *(continued).*

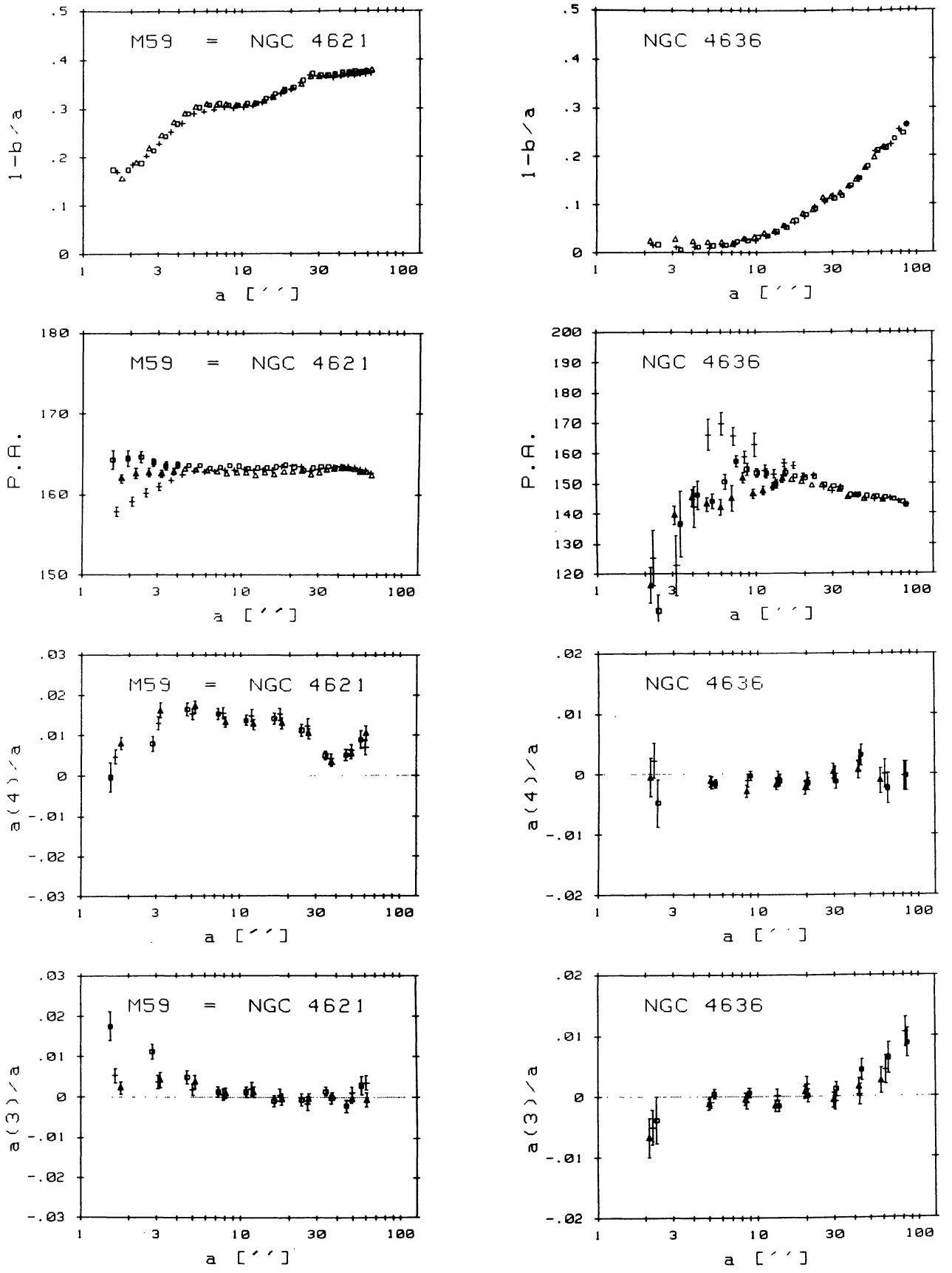

FIGURE 13 *(continued).*

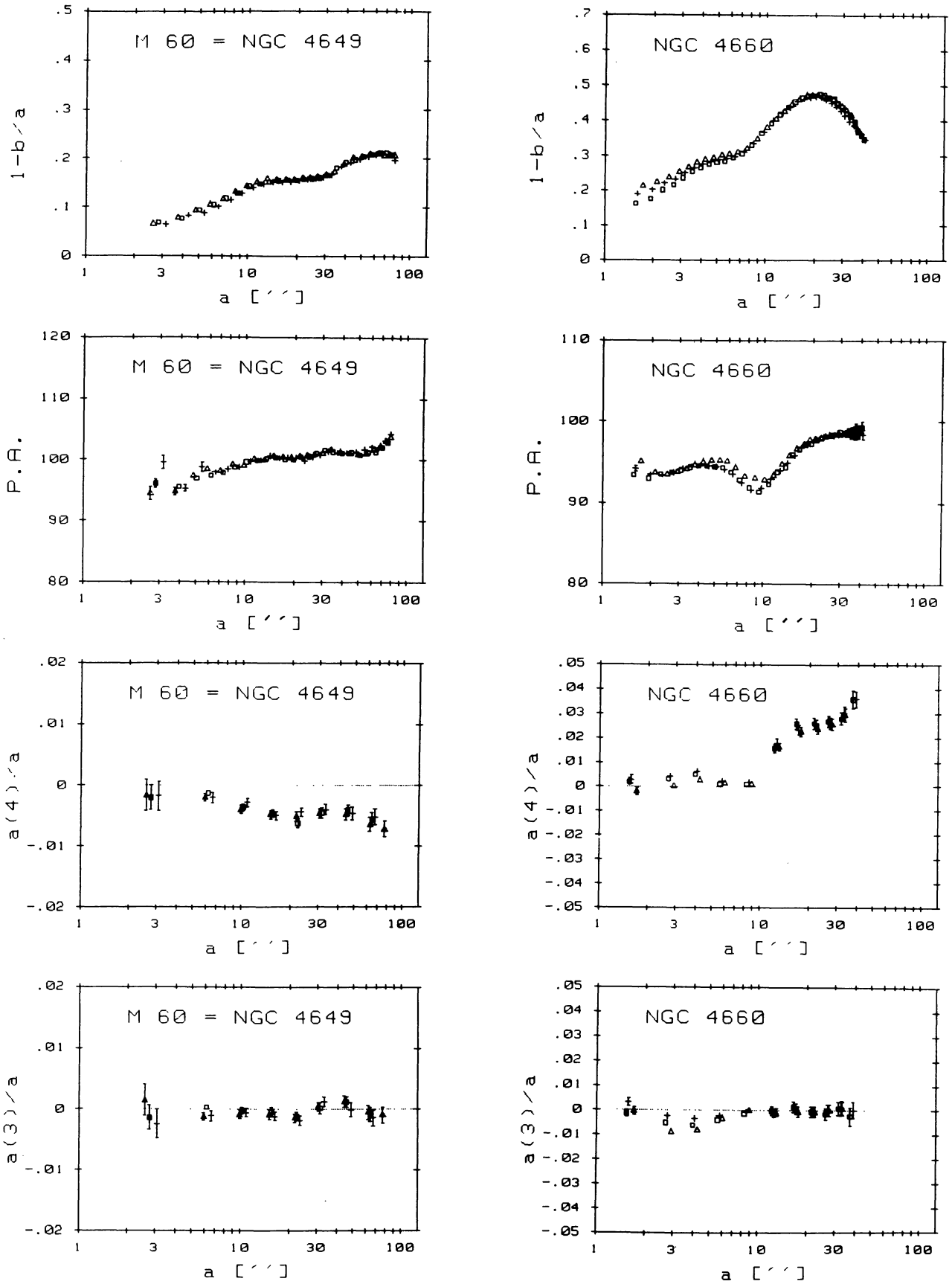

FIGURE 13 *(continued).*

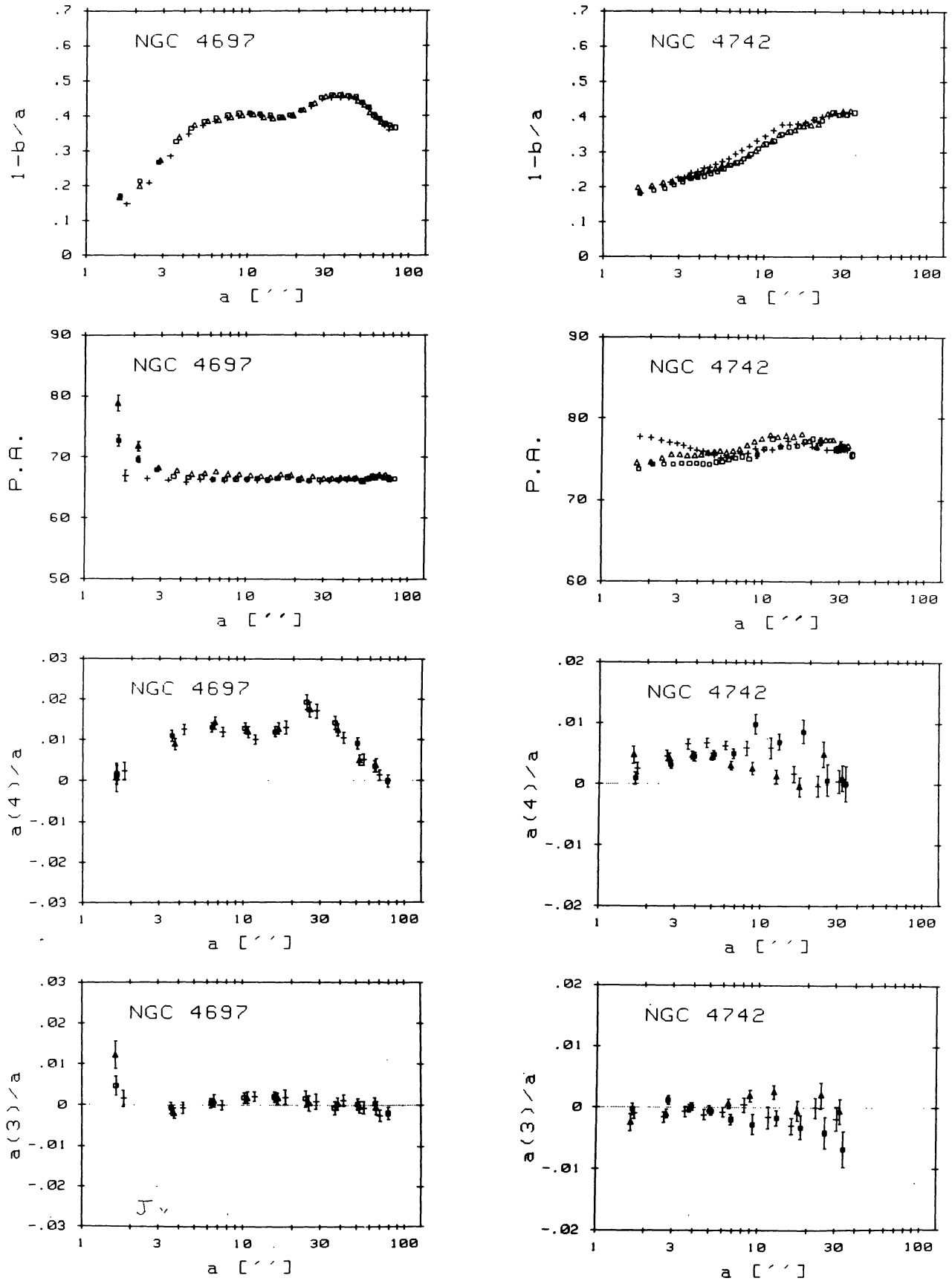

FIGURE 13 *(continued).*

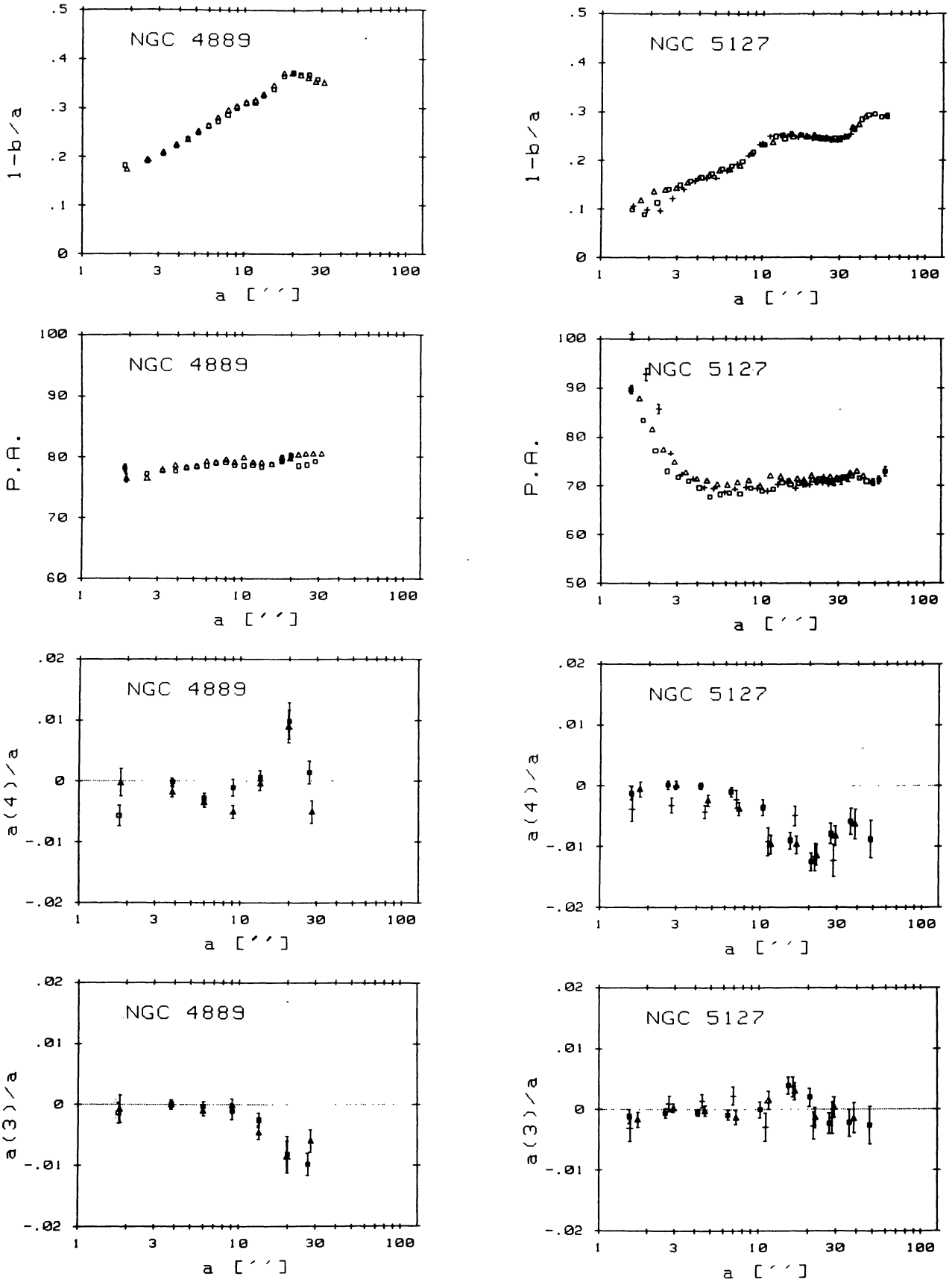

FIGURE 13 *(continued).*

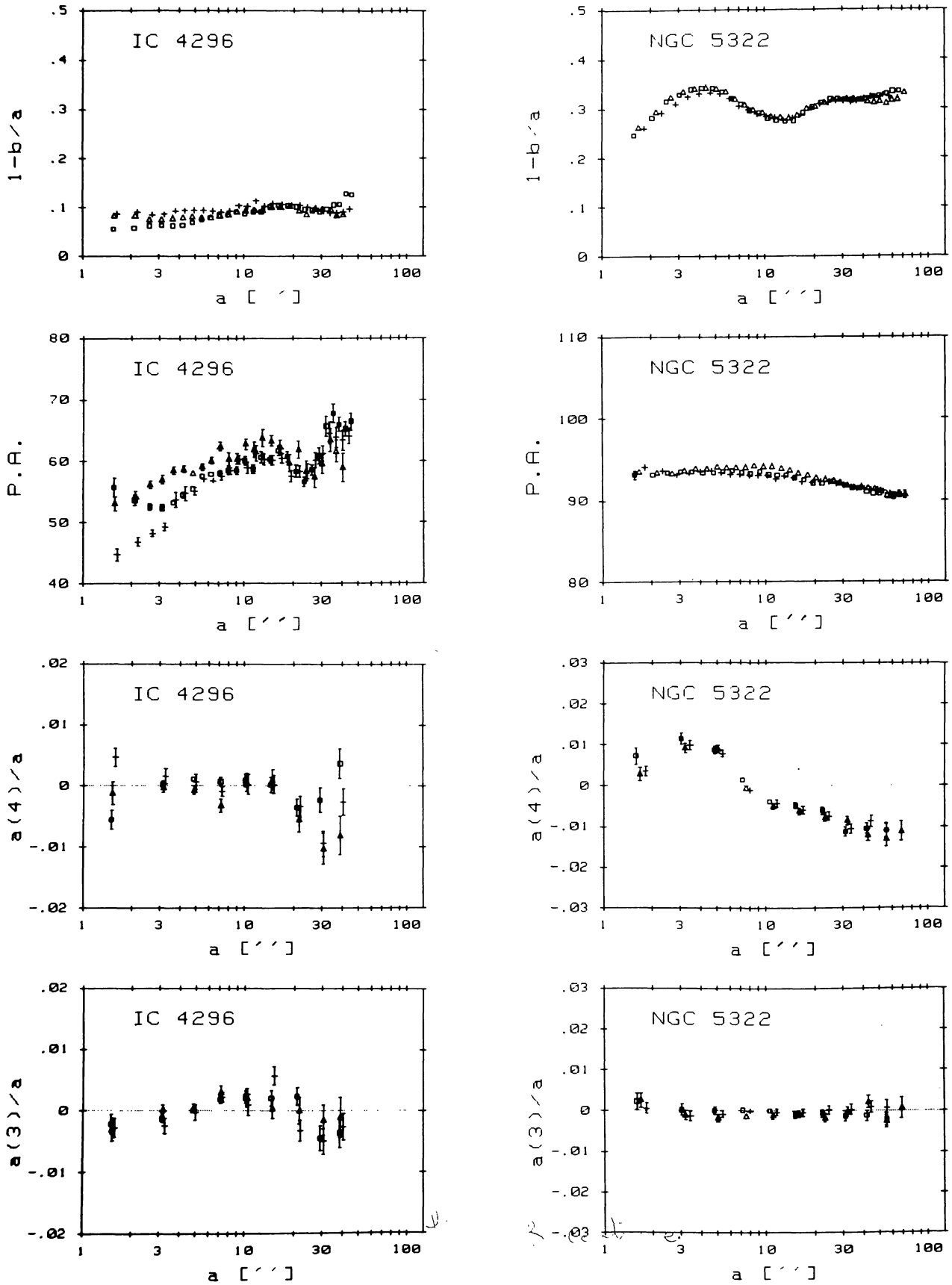

FIGURE 13 *(continued).*

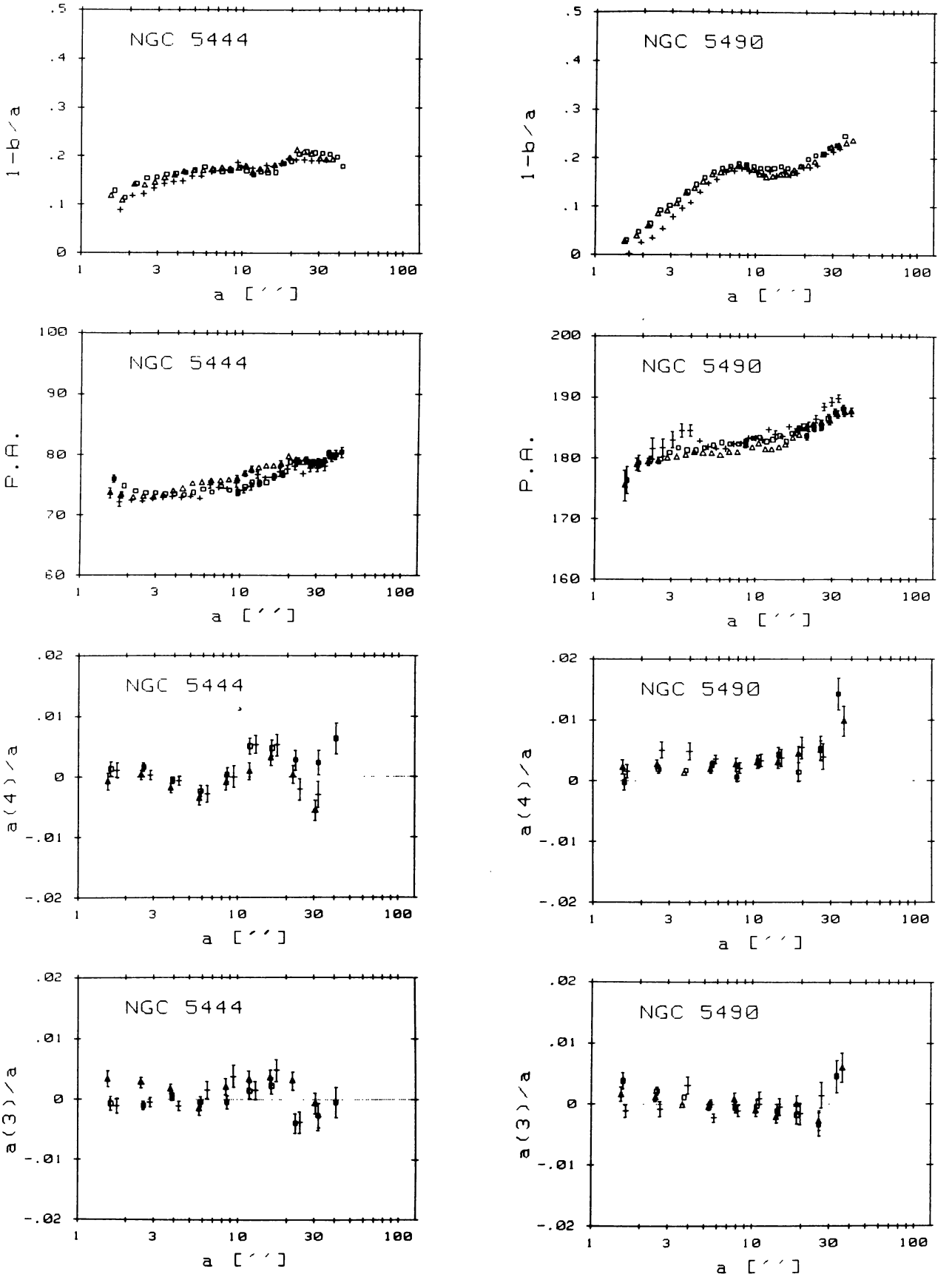

FIGURE 13 *(continued).*

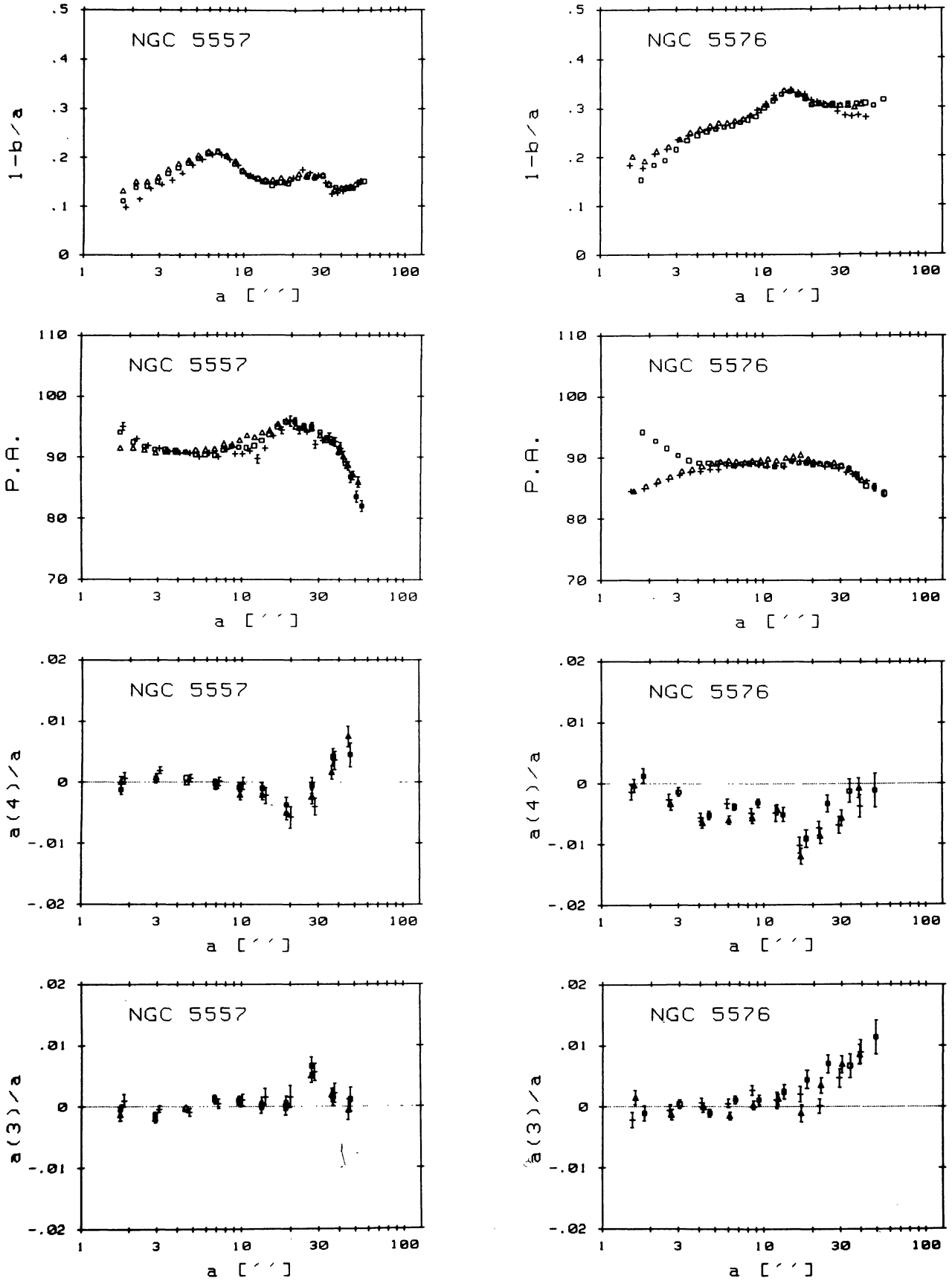

FIGURE 13 *(continued).*

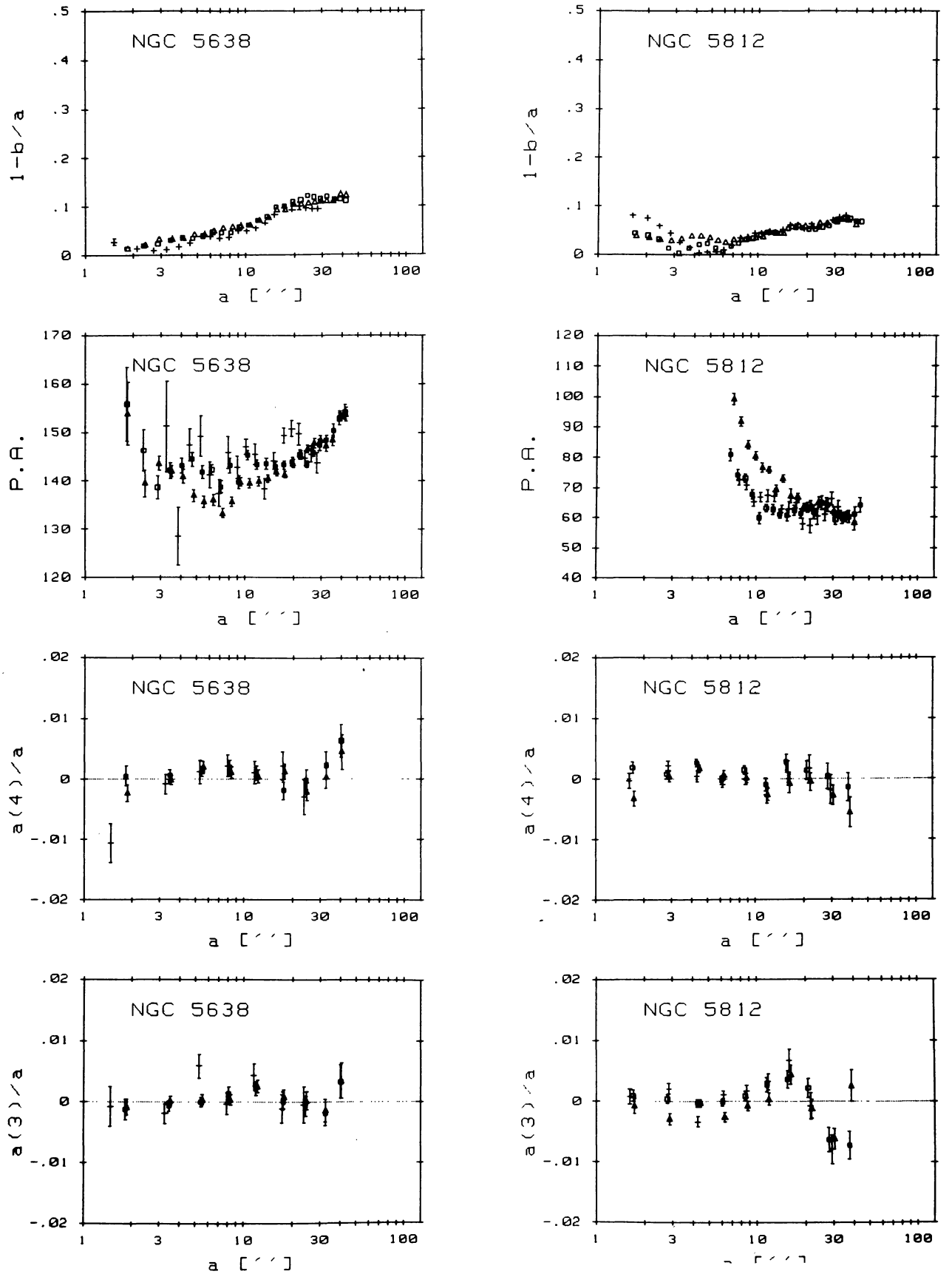

FIGURE 13 *(continued).*

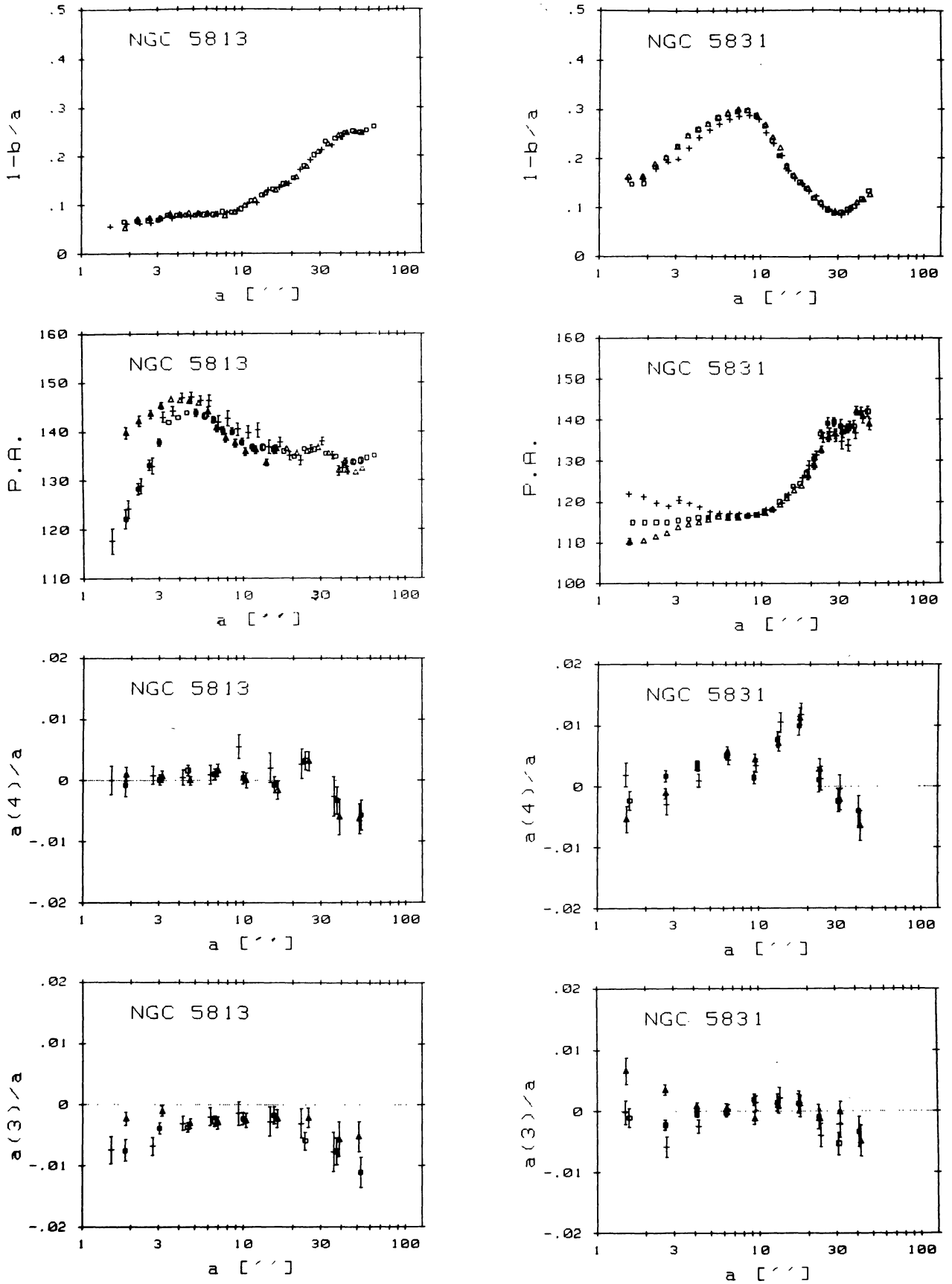

FIGURE 13 *(continued).*

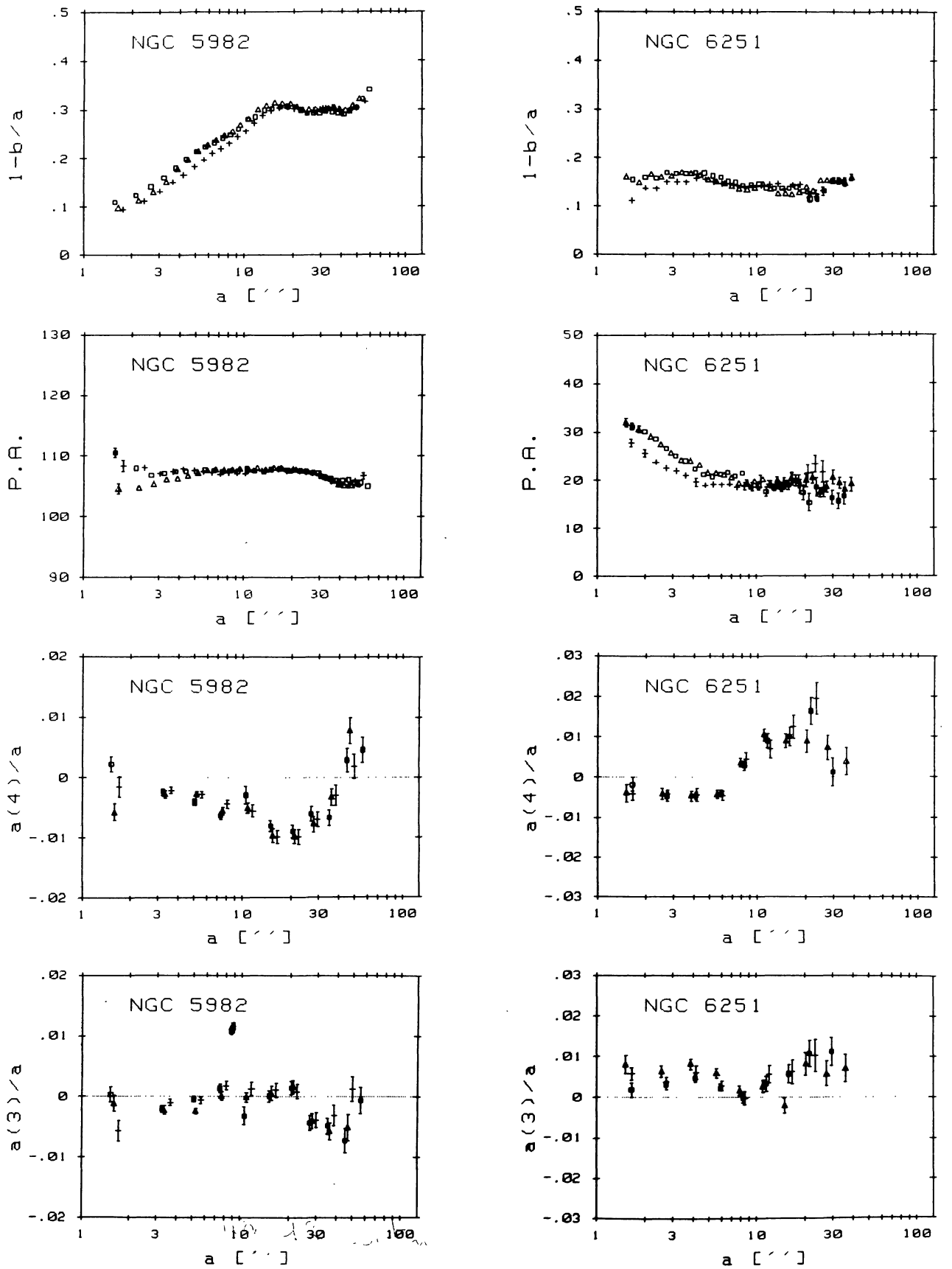

FIGURE 13 *(continued).*

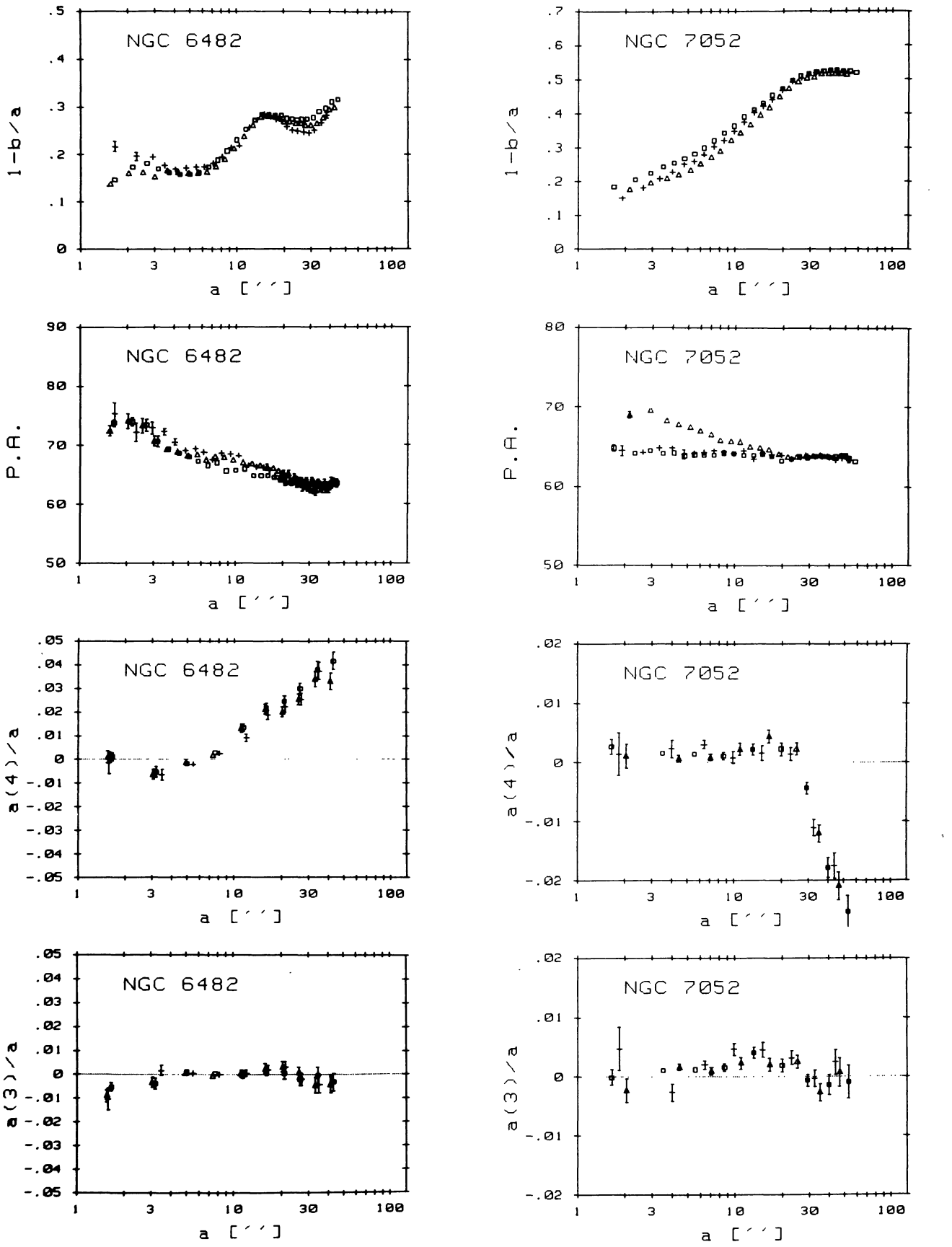

FIGURE 13 *(continued).*

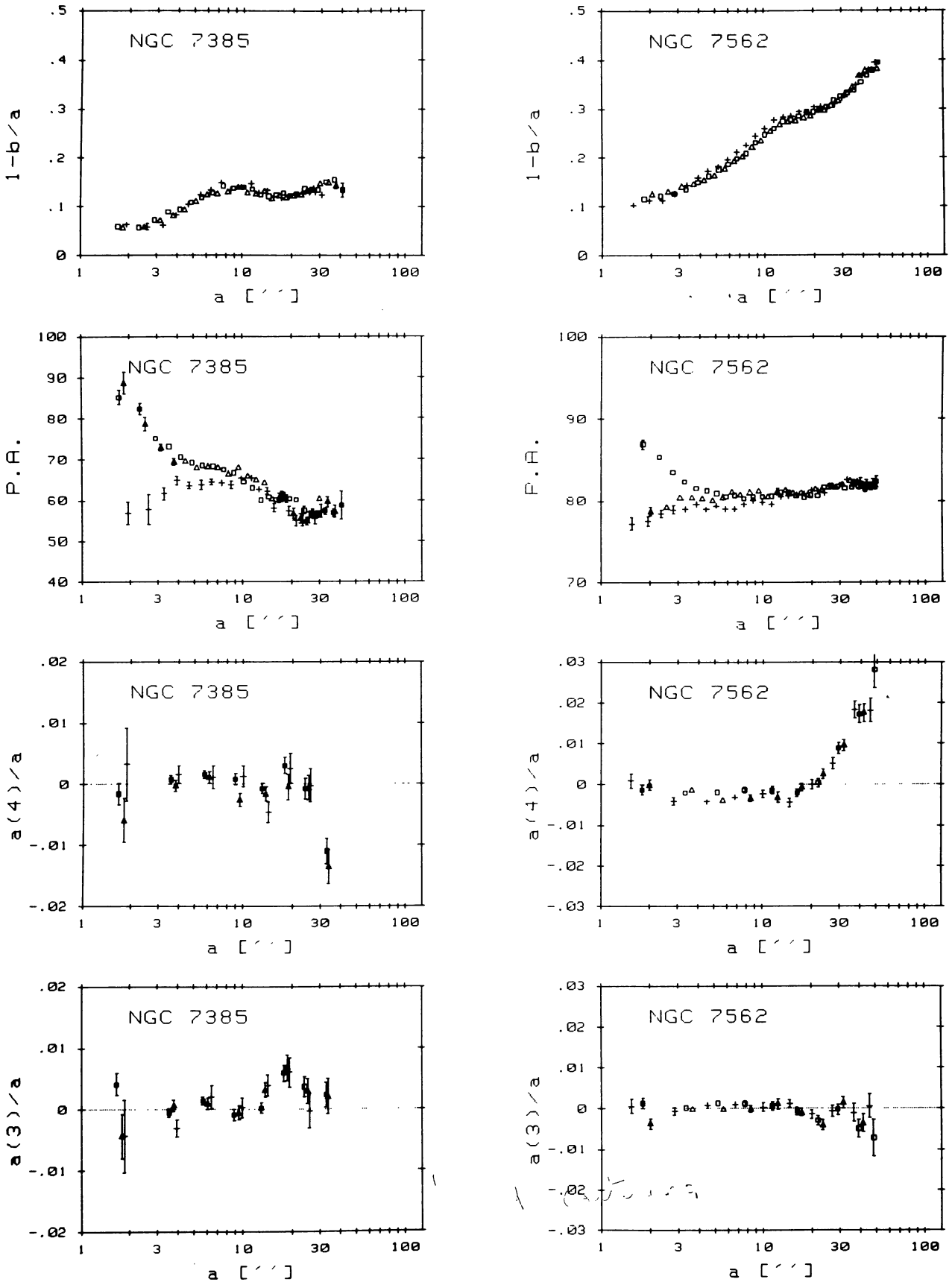

FIGURE 13 *(continued).*

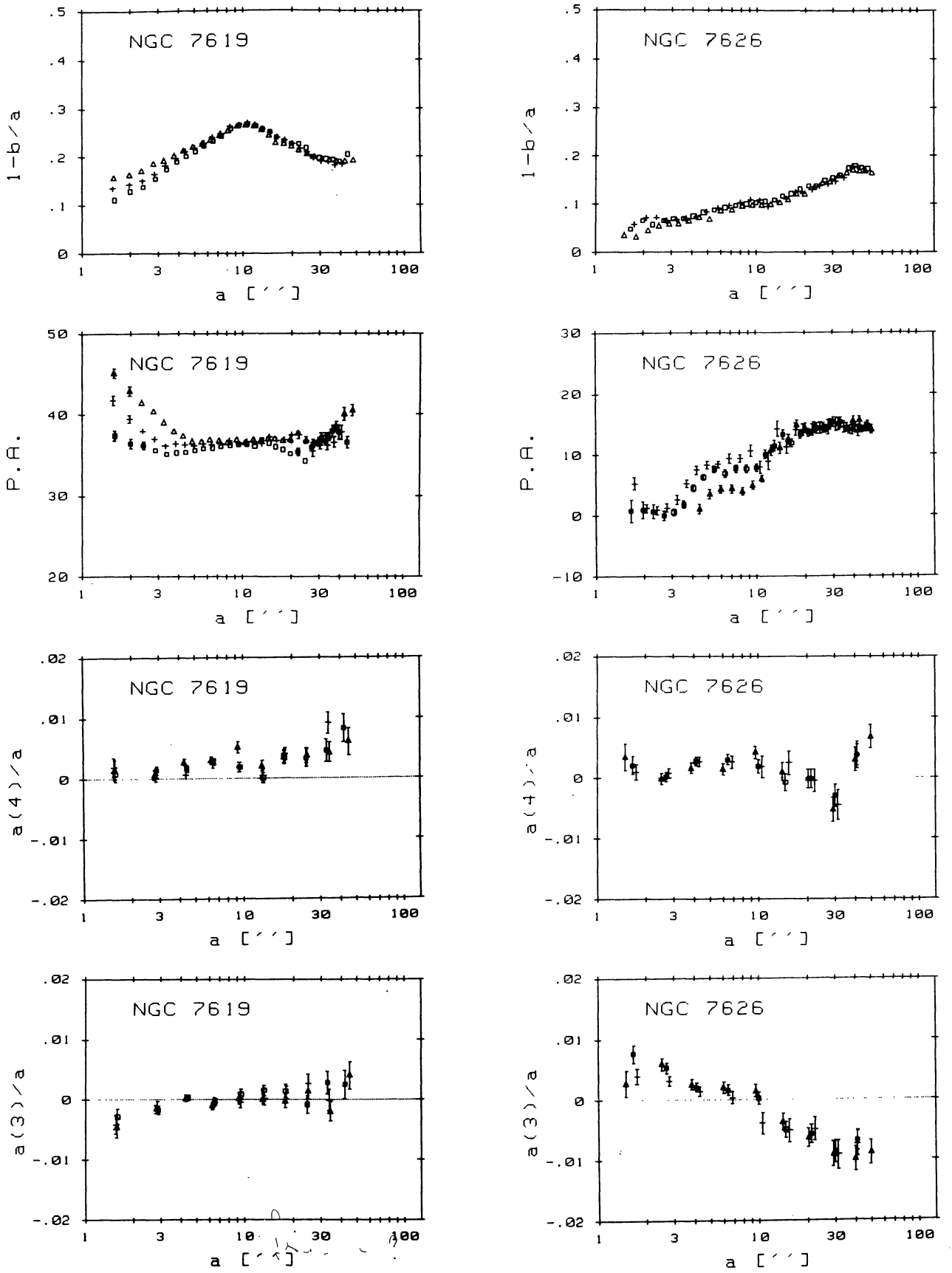

FIGURE 13 *(continued).*

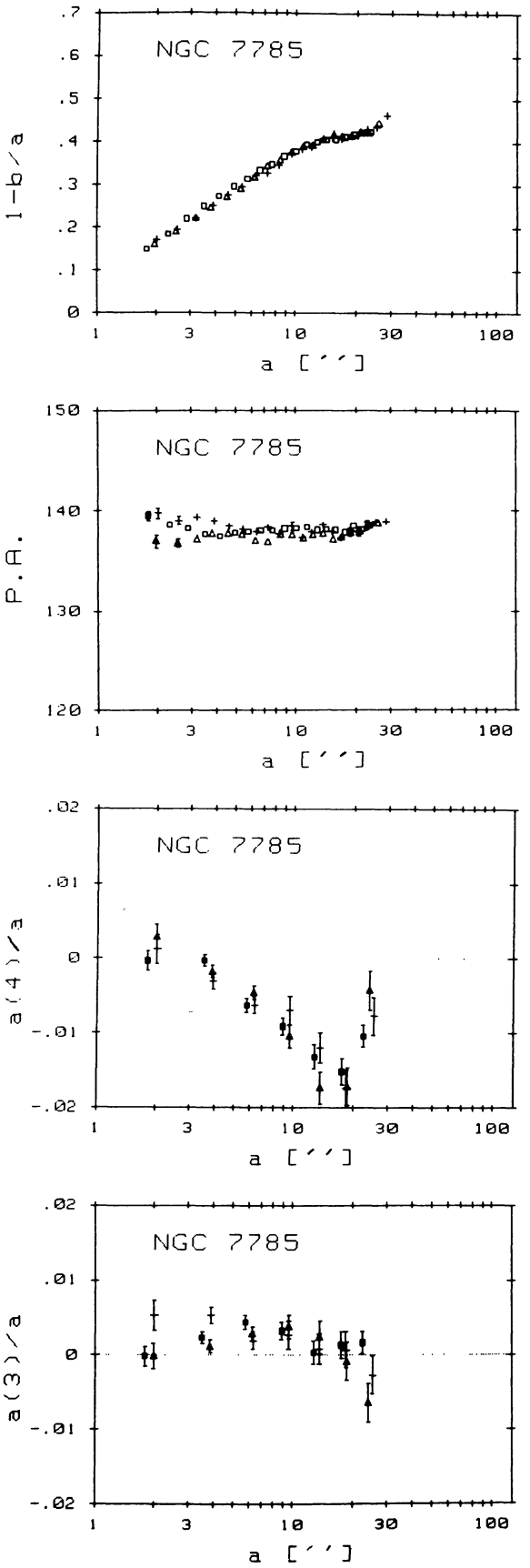

FIGURE 13 *(continued).*